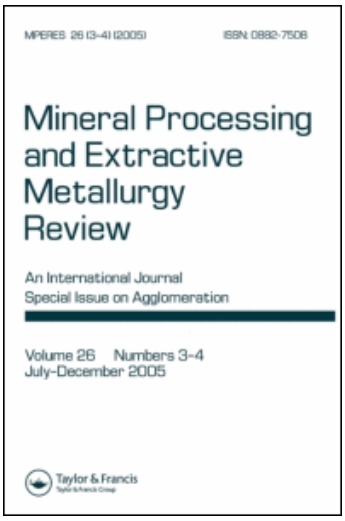

Mineral Processing and Extractive Metallurgy Review
Publication details, including instructions for authors and subscription information:
http://www.informaworld.com/smpp/title~content=t713644625

Development of Beryllium Single Crystal Material for Monochromator Applications

F. Mücklich [a]; G. Petzow [a]
[a] Max-Planck-Institute of Metals Research Stuttgart, Institute of Materials Science, Powder Metallurgical Laboratory, Stuttgart, Germany

Online Publication Date: 01 November 1994

To cite this Article Mücklich, F. and Petzow, G.(1994)'Development of Beryllium Single Crystal Material for Monochromator Applications',Mineral Processing and Extractive Metallurgy Review,13:1,193 — 227
To link to this Article: DOI: 10.1080/08827509408914111
URL: http://dx.doi.org/10.1080/08827509408914111

Mineral Processing and Extractive Metallurgy Review
1994, Vol. 13, pp. 193–227
Reprints available directly from the publisher
Photocopying permitted by license only

Development of Beryllium Single Crystal Material for Monochromator Applications

F. MÜCKLICH and G. PETZOW

Max-Planck-Institute of Metals Research Stuttgart, Institute of Materials Science, Powder Metallurgical Laboratory; Heisenbergstraße 5, D-7000 Stuttgart 80, Germany

Beryllium offers a unique combination of properties for the development of extraordinary scattering behavior. Therefore, many different potential applications call for an advanced material based on Beryllium. This paper summarizes something of today's knowledge about crystal growth behavior and the role of defect structures for the control of different scattering properties in this metal. While we are still at the beginning of true "defect structure design", which demands further theoretical and experimental investigation, Beryllium—also in the single crystal state—offers unique potential, if it can be developed for the achievement of custom tailored properties by proper control of the defect structure.

Key words: defect distribution; deformation; dislocation; monochromator; mosaic crystal; mosaicity; polychromatic beam; synchrotron beam

INTRODUCTION TO BERYLLIUM PROPERTIES RELATED TO THE BASIC REQUIREMENTS OF MONOCHROMATOR CRYSTALS

Among the special properties of Beryllium are extraordinary combinations of attributes which emphasize its unique potential as a monochromator material for neutrons as well as for synchrotron radiation. Figure 1 shows the most relevant of the physical properties and indicates their importance for the different applications. The use of Beryllium single crystals as the most favorable material for monochromatization of neutron spectra had been proposed primarily due to the combination of a high coherent cross section for neutrons with an incredibly low attenuation of the neutron beam by capture, incoherent and inelastic scattering processes. This means that the neutrons will penetrate the lattice with low attenuation until they reach their individual depth for the Bragg reflection. Due to the high coherent cross section the necessary reflecting depth of the Bragg position is only a few millimeters and decreases with increasing structure factor of the reflection. Therefore, the intensity output should be the highest of all materials. Nevertheless for assumptions of absolute reflectivities, extinction and multiple scattering effects must be taken into account /1, 2/. Additionally, for short wavelengths the spectrum should also be relatively "clean", because the disturbance by parasitic reflections is much less due to the small lattice distances in Beryllium. Finally,

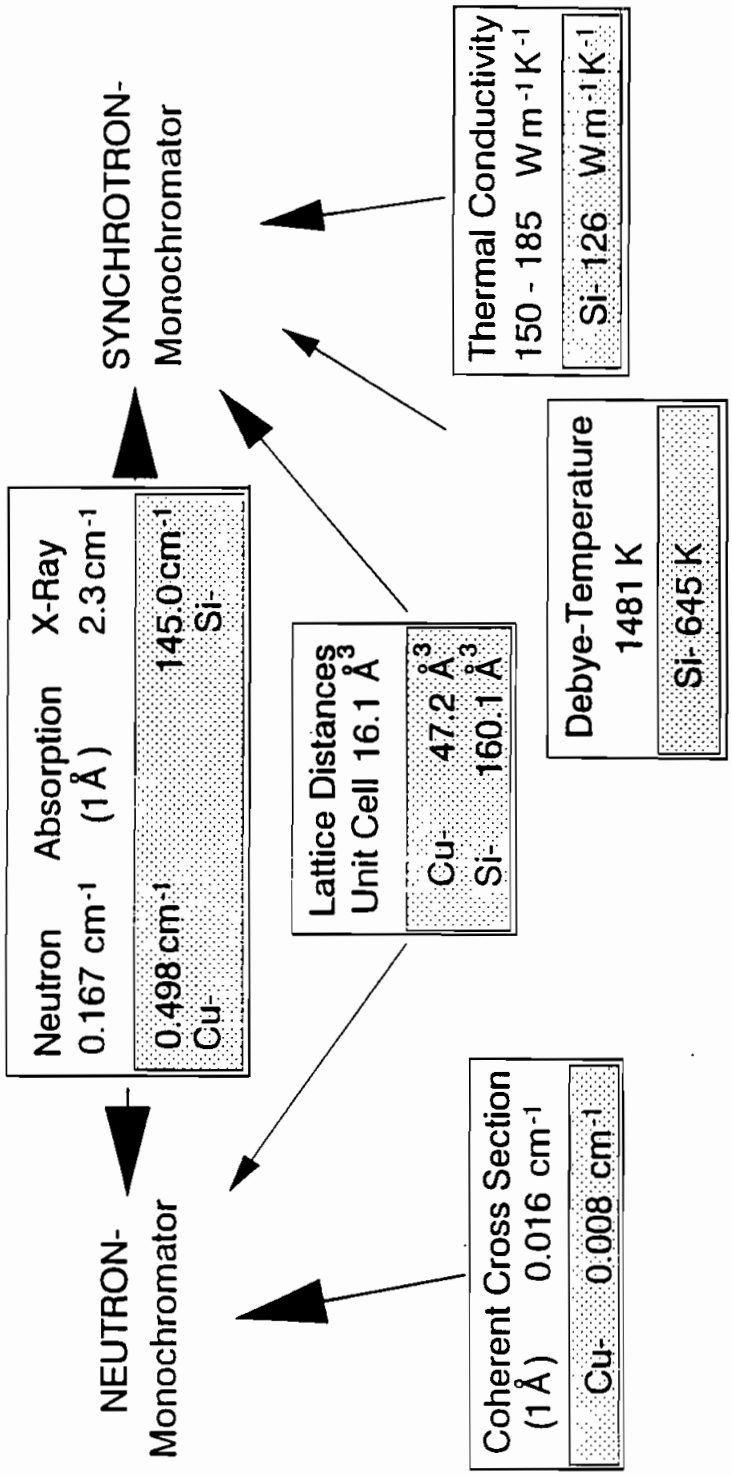

FIGURE 1 Physical properties related to the scattering behavior of Beryllium.

considering the Bragg equation, the smaller lattice distances lead to higher Bragg angles which are useful for exceptional resolution functions even with higher neutron energies.

In order to discuss Be as a monochromator material for synchrotron radiation, it is necessary to consider the specifics of X-rays as a form of electro magnetic radiation. Although the atomic number is low and therefore the number of scattering electrons per atom, Beryllium can still be an efficient monochromator also for electro magnetic radiation. The Bragg intensity of the elements increases for X-rays with the second power of the atomic number but the intensity loss by absorption, in general, increases with the third power of the atomic number. In the case of Beryllium, this leads to a high, and therefore, advantageous ratio of scattering power to absorption /3, 4/. In other words, this means the penetration depth of the beam is controlled by the elastic scattering. The Debye temperature of Beryllium is one of the highest in the whole Periodic System, and is over twice as big compared to all the other elements with the exception of carbon. This is also connected to an especially high value of specific heat and leads to a very low oscillation effect of the atoms caused by the introduced heat from absorption of electromagnetic waves. This occurs in addition to the extremely low absorption mentioned above. A very high thermal conductivity enables the efficient cooling of every monochromator element and the low coefficient of thermal expansion compared to high thermal conductivity reduces the lattice deformations produced by thermal gradients. Last but not least, the low values of lattice distances lead, in this case also, to useful high Bragg angles and therefore improved resolution functions in the scattering geometry.

"Ideal" Real Structure Design of Mosaic Monochromator Material

There are a number of structural properties that an ideal mosaic monochromator should have. Firstly, the lattice should have the properties of an ideal mosaic crystal. The assumptions of this model are never fulfilled completely in real non-perfect crystals. Nevertheless we will stress this model in order to give ideas for the final destination of materials science in this field, but it is still a well known problem in crystallography to find an adequate description for the diffraction process in the real non-perfect crystals.

The ideal mosaic crystal means a homogeneous distribution of the orientations of so called mosaic blocks. The size of these mosaic blocks, assumed to be undisturbed volumes, should be smaller than the extinction length. In this case we can neglect the screening of interference by deeper lattice regions of the coherent scattering volume and kinematic theory can be applied /5/. On the other hand the orientation distribution of these mosaic blocks should be of the Gaussian type. If this is fulfilled, the crystal is in the Bragg position for all beams of the given divergence and can reflect with maximum intensity for the wavelength, chosen by the Bragg equation. The selected bandpass is given by the "uncertainty" of the distance and orientation of the reflecting lattice planes respectively. Therefore the mosaic distribution function is an important parameter which is deeply connected with the real structure of the crystal lattice and the Bragg reflections /6, 7, 8/. Mosaicity itself means the orientation distribution density of the individual mosaic

blocks and can be measured directly as the rocking curve in γ-ray diffractometry /9, 10/. In this case the mosaicity is represented mainly by the parameter FWHM (Full Width at Half Maximum) of the orientation distribution density.

For applications in neutron scattering the mosaicity should have values between 20 and 40 minutes of arc in order to optimize monochromatic intensity and wavelength bandpass. For most of the synchrotron applications the mosaicity should preferably be smaller than one minute of arc because the radiation has a high brilliance with an extremely small primary divergence. The consequence of this are much smaller monochromator dimensions of only a few square millimeters /4, 11/ compared to between 130 and 200 square centimeters for the monochromatization of neutrons /8, 12/.

GROWTH PECULIARITIES OF BERYLLIUM SINGLE CRYSTALS

The extraordinary combination of properties displayed by Beryllium calls for some non conventional techniques for growing single crystals of high lattice perfection. Many attempts have been made with techniques like slow solidification of molten Be in a crucible, direct crystallization from the vapor phase or Czochralski and Bridgman techniques. The most successful techniques were found to be the cruciibleless growth in a mirror furnace /13/. Figure 2 shows the scheme of a double ellipsoid mirror furnace for growing crystals with diameters up to 15 mm. The oriented seed and the polycrystalline starting material can be rotated and translated independently in order to allow a necking process. The Beryllium material grows in a quartz tube which is evacuated and filled with Argon to reduce the evaporation of Beryllium from the heated and molten material. The furnace consists of a set of elliptical mirrors each with a halogen lamp mounted at one of its focal points. The Beryllium crystal is positioned in the other focal point common to all the elliptical mirrors. This growth technique has the following advantages:

—no "forced doping" by the crucible material and its impurities, which is important due to the low solubilities of most elements in Beryllium
—no sticking to the crucible wall during solidification and cooling
—no secondary nucleation starting from the crucible wall.

On the other hand there are special disadvantages of such a growth technique compared to the Bridgman- or Gradient Freeze techniques.

—high temperature gradients in axial, radial and azimuthal directions
—no direct control of these gradients

Therefore some crystal growth studies have been undertaken in order to increase the reproducibility and the perfection of the crystal lattice.

Crystal Growth Studies

To increase the perfection of the crystal lattice requires initially reaching a stable level of reproducibility of the crystal growth process. For this purpose some of the

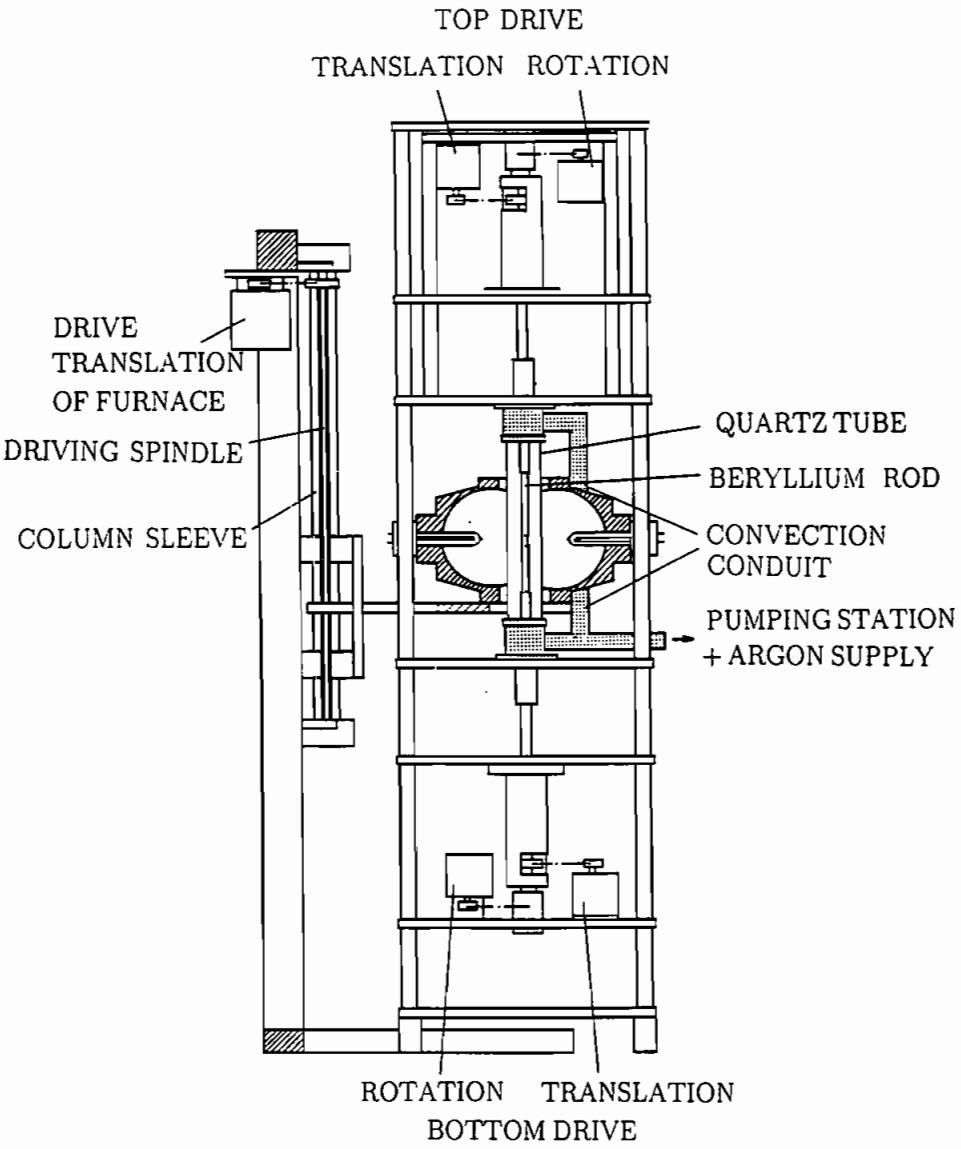

FIGURE 2 Scheme of a crucibleless mirror furnace /13/.

obviously important influences like that of vibrations on the misorientation of subgrains, the correlation of the crystal symmetry and the symmetry of temperature field, convection influences in the melt and some impurity influences have been investigated in some detail and will be discussed below.

The ways of enhancing the perfection of the crystal lattice are expected to be largely connected to the availability of a super pure starting material and investigations for the control of temperature fields during solidification as well as during

the β-α-Transformation and cooling process /14, 15/. Some of the first results will be presented in the following paragraph.

To increase the reproducibility of the crystal growth process fig. 3 shows the typical shape of the free grown crystals. Periodic surface structures reflect the oscillations in the solidification process. The characterization of these surface structures allows us to draw some conclusions about the influences of the growth process itself. Figure 4 shows a logarithmic plot of the surface amplitude versus its characteristic frequency on the surface, considering the growth velocity. The frequencies above 0.1 Hz lie on a straight line which is given by the oscillation system of the molten Beryllium zone. The lower frequencies have amplitudes below this line because the operator may act as a "damper". The three different rotation velocities (0.022–0.1 Hz) are obviously presented on the surface as well as the frequency of AC (50 Hz). Between these, the resonance frequency of the molten zone can be found but also the resonance frequencies of the growth facility. Therefore these measurements have been a valuable tool for the elimination of disturbing vibrations in the crystal growth process /15/.

An influence on crystal growth behavior also comes from the interaction of crystal symmetry of the hexagonal Beryllium lattice and the symmetry of the temperature field. Typical growth directions are $<11\bar{2}0>$ or $<10\bar{1}0>$. In these cases a twofold crystal symmetry is also combined with a "twofold" symmetry of the temperature field. Under these circumstances the stability of the growth of different lattice planes will be connected to parameters such as the "smoothness" of these planes. Its physical base is the periodic repetition of surface energies with the lattice

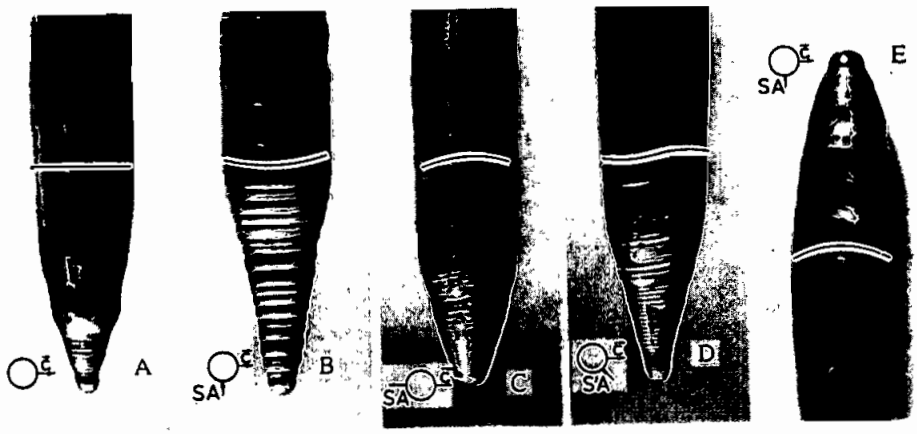

FIGURE 3 Typical shape of Beryllium single crystals, grown under different angular positions of c-axis to the symmetry axis of the heating system. Note the different shape of the surfaces due to striation development.

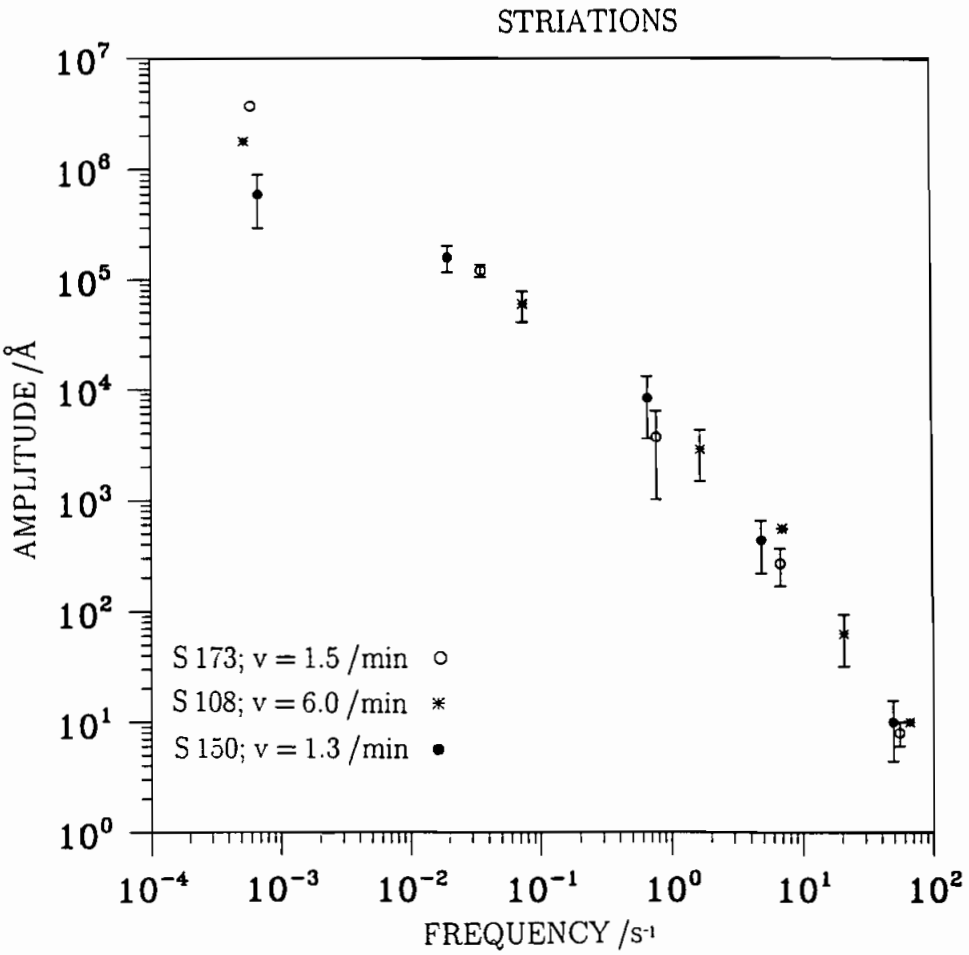

FIGURE 4 Logarithmic plot of surface oscillations along the crystal growth axis versus its characteristic frequency on the surface, considering the growth velocity. The different signs represent three different rotation velocities during solidification (see text).

distance. The deposited growth layer contains a high frequency of bondings. The frequency between these layers is rather small. Under certain preconditions (PBC model /16/) this encourages the lateral growth of lattice planes with high frequencies of bonding and moderates the growth velocity perpendicular to these lattice planes /16/. Following this model the smoothness of lattice planes increases with increasing relative frequency of bonding within a lattice plane /16/. This also leads to an anisotropical behavior of thermal conductivity as well as to an anisotropical crystallization. If the growing crystal is rotating with a certain velocity under these symmetry conditions time dependent changes in crystallization behavior and therefore in the crystal perfection have to be taken into account.

On the other hand, changes in the rotation conditions will drastically modify the convection characteristics in the melt. For conventional zone melting processes

with rotating melting and solidifying material, the convection state is driven by gravity (Rayleigh number), the surface tension (Marangoni number) and the rotation itself (Reynold number), while for a non-rotating system the convection is determined by the Rayleigh number alone. In this case, for the given melt it depends on height to diameter ratio of the molten zone as to whether the convection is steady or unsteady /17/.

Besides this principle discussion a simple experiment shows the consequence of different crystal orientation towards the symmetry of the heating system /15/. To demonstrate this the conventional rotation of the crystal was stopped and the seed was oriented in three crystallographic positions (fig. 5). The orientation is given as the angle between the c-axis of the crystal and the axis connecting the two lamps of the mirror furnace. The striations, visible on the surface of the crystal, clearly

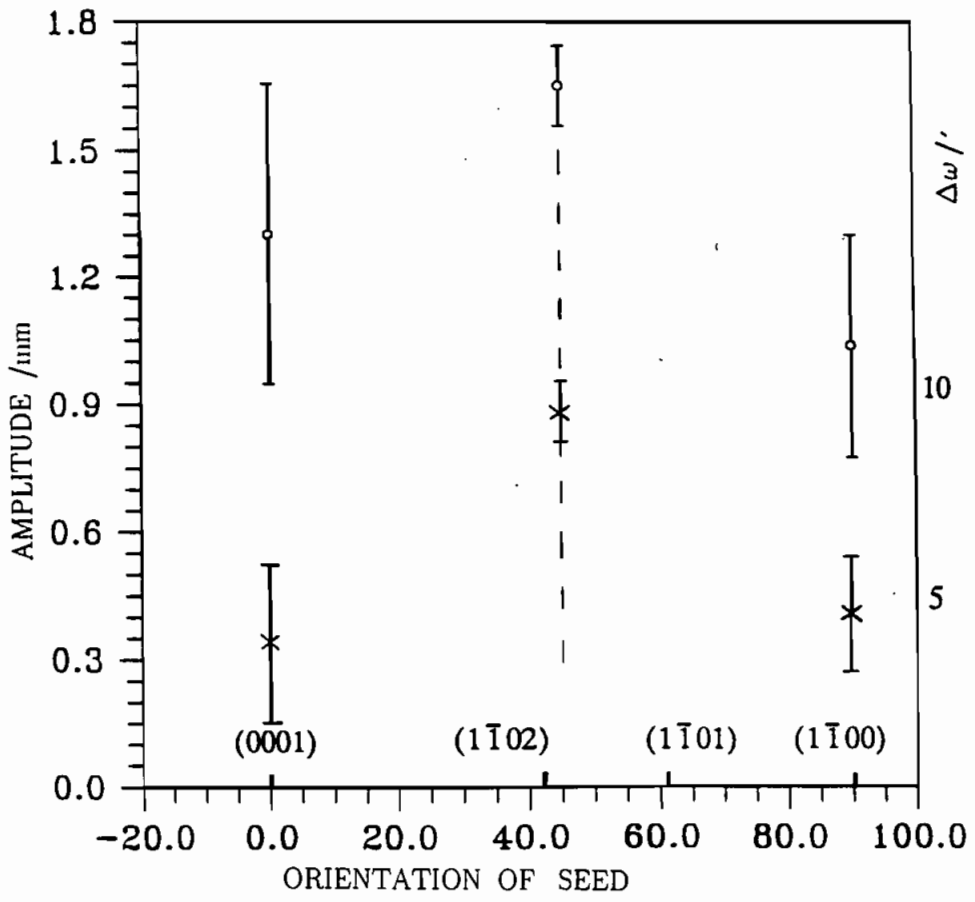

FIGURE 5 Influence of different orientation of the seed towards the symmetry of the heating system. The orientation is given as the angle between the c-axis of the crystal and the axis connecting the two lamps of the mirror furnace. The left ordinate shows the influence on the amplitude of curvature of the striations (o), (see also fig. 3). The right ordinate indicates the connection to the misorientation of subgrains, measured with the γ-ray diffractometer (X).

bent due to the non radial thermal distribution. The interesting fact is that the amplitude of this curvature depends on the crystal direction. This supports the strong influence of the previously mentioned anisotropy of thermal conductivity. The left ordinate shows the influence on the amplitude of curvature of the striations (see also fig. 3). There is a significant maximum in the amplitude for the case of a high indexed lattice plane lying orthogonal to the lamps axis. This confirms that it has a relatively low thermal conductivity (due to lower bonding frequencies) and therefore travels faster ahead of the solification front. The right ordinate indicates the connection to the misorientation of subgrains, measured with the γ-ray diffractometer. In every experiment near this maximum in the striation deformation amplitude the misorientations of subgrains have exceeded 9 minutes of an arc, or even the whole crystal grew polycrystalline, whereas for the low indexed orientations the misorientations did not exceed 7 minutes of arc and every growth experiment has been successful.

As mentioned above, such experiments can only be performed if the material fulfills the precondition of high purity. It is well known that most of the elements have a rather low solubility in the Beryllium lattice and therefore critical enrichments probably should lead to precipitations and consequently to the formation of subgrain boundaries. Nevertheless evidence for significant impurity enrichments in the subgrain boundaries must be given: The typical available original material has impurity concentrations of oxygen and different kinds of metal atoms summarily exceeding 1000ppm and is therefore unsuitable for single crystal growth. Hence it must be cleaned by an extensive zone refining e.g. from 20 to 40 passes. Afterwards the impurity concentrations are typically below 200ppm. With residual resistance measurements, with local resolution of four points along the Beryllium rod, quick and nondestructive information about impurity distributions along the purified rod can be extracted /14/. Figure 6 shows that single crystal growth is always successful only above a critical region of resistivity ratios from 8 to 12. Obviously there is some correlation between the concentration of dissolved impurity atoms (which are most effective for residual resistivity) and precipitated concentrations, which should be most effective for the formation of subgrain boundaries. To verify the role of impurities for subgrain boundary formation the concentration of impurities was studied in the vicinity of subgrain boundaries. While conventional techniques failed in this high purity material only the spectra of Rutherford Back Scattering technique (RBS) has been able to measure significant concentrations of impurities, notably Oxygen and Iron (fig. 7). This method takes advantage of the much higher atomic weight of all the relevant impurity atoms compared to the light Be host atoms and thus exhibits an especially high sensitivity for this case /14/.

After such measurements target preparations of subgrain boundary regions were examined using transmission electron microscopy in order to determine the microscopical behavior of these impurity concentrations. Figure 8 shows a typical precipitation composed of Cr, Ti, Al and Si which is touched upon by the dislocations of the subgrain boundary. The shift of corresponding Kikuchi lines indicated the weak misorientation connected with this boundary. No scattering pattern of the precipitation could be achieved to clarify its crystalline nature. Obviously they have a rather inhomogeneous nature and their effect could be dominated by the simple difference in thermal expansion.

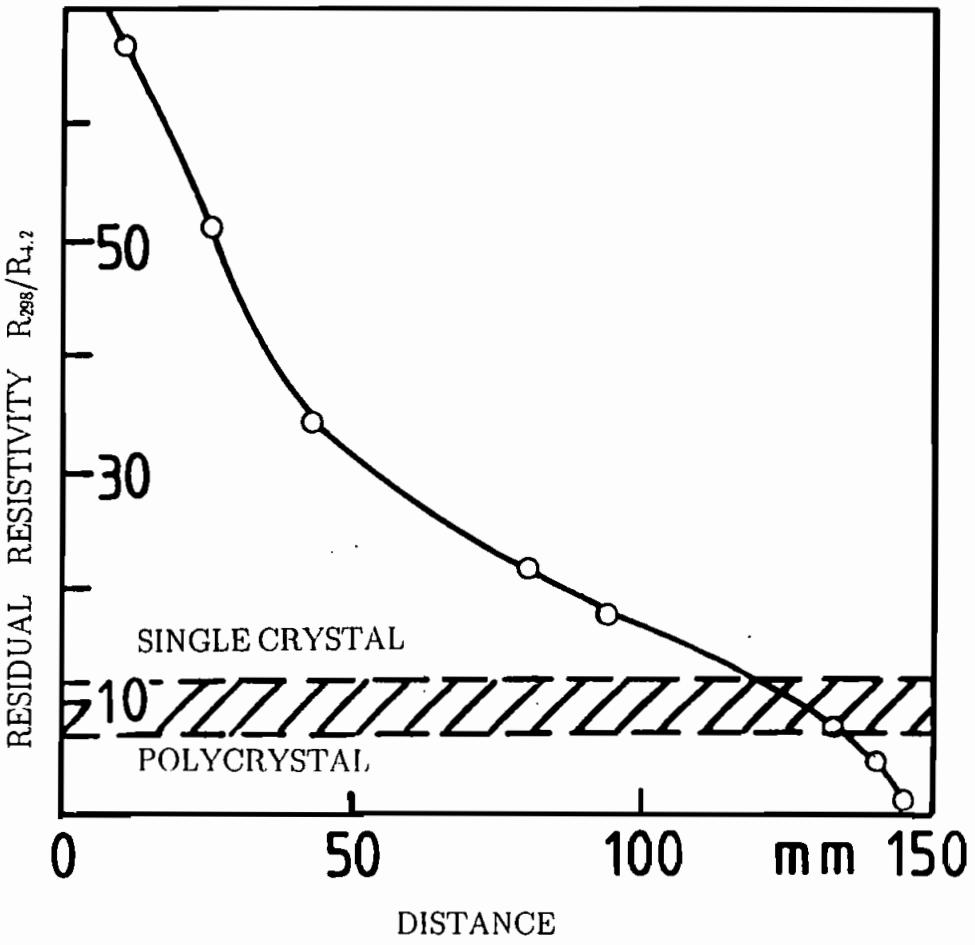

FIGURE 6 Residual resistivity measurements along Beryllium rods purified by zone refining. The critical resistance ratio for the breakdown of single crystal growth is shown and indicates a correlation of the concentration of soluted impurity atoms which are most effective for residual resistivity, and precipitated concentrations which should be most effective for the formation of subgrain boundaries.

Another group of precipitates has a high content of Al and Mn. They have been found especially in the volume of individual subgrains (fig. 9). These precipitates are obviously of a coherent type and show additional reciprocal lattice points between the host lattice. Though the nature of these precipitations might be interesting, no interaction with dislocations are visible in contradiction to the other type shown in fig. 8 and their role for the formation of subgrain boundaries should be negligible.

To learn something about the local origin of these precipitation effects it is interesting to look more closely to the local inhomogeneities of impurity concentrations. Therefore the connection to striation formation has been studied. Figure 10 shows the principle manifestation of striations as a spiral line if the crystal is

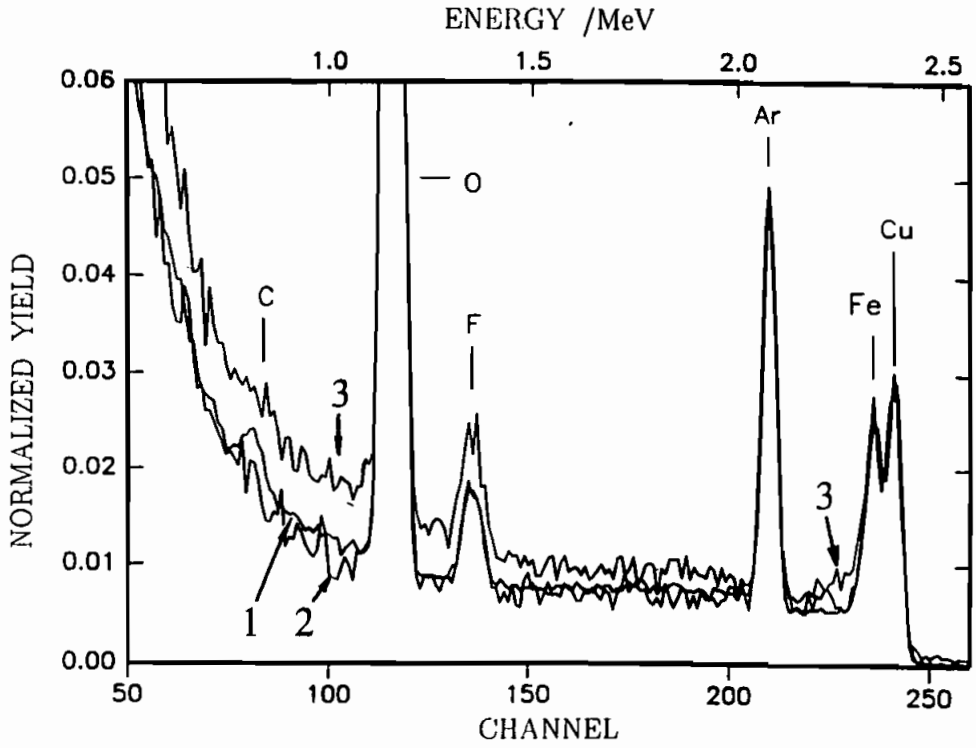

FIGURE 7 Rutherford Back Scattering (RBS) spectra of 3 MeV Helium ions generated directly at the subgrain boundary region (3) in comparison to the adjacent subgrains (1,2). The difference of the spectra shows significant concentrations of impurities such as oxygen and iron in the grain boundary, more than twice as high as in the individual subgrains /14/.

cut perpendicular to the growth direction. Again by RBS impurity concentrations have been measured along the radius of the polished surface. Local enrichments of impurities coincide with the striation line (fig. 10). It can be assumed that these striations play a stimulating role in predetermination of subgrain boundary formation because they support local high concentrations of impurities even if the material is rather poor, i.e. if the overall concentration of impurities appears to be uncriticially low. Therefore the solidification mechanisms which interact with shape and sharpness of striations should be considered /15/, particularly the supercooling which influences the oscillation of impurity concentration along the growth direction. Therefore investigations of controlling parameters of supercooling such as growth velocity and temperature gradients at the solidification front might be useful to understand these interactions and to reduce local impurity concentrations.

One of the many interesting pecularities of the element Beryllium is the lattice transition from b.c.c.-A2 to h.c.p.-A3 very close to the melting point (transition temperature 1527 K, melting point 1560 K) connected with the highest of all transition enthalpies and nearby the melting enthalpy (transition 6849 kJ/mol, melting 7895 kJ/mol) /18, 19, 20/. This transition exhibits a volume effect of

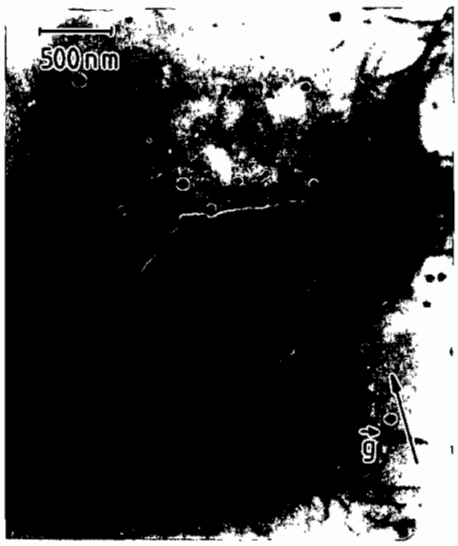

FIGURE 8 Typical precipitation at the subgrain boundary with dominating contents of Chromium and Titanium but also Aluminium and Silicon. The TEM-imaging indicated a weak misorientation between the upper left and lower right region by a shift of the corresponding Kikuchi lines. Small dark points are residual enrichments of Copper caused by spark erosion.

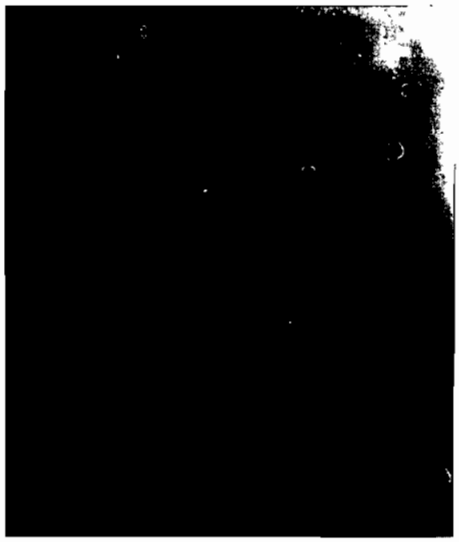

FIGURE 9 Hexagonal precipitations with high contents of Aluminium and Manganese. These precipitations show a coherent incorporation in the host lattice with nearly the double value of lattice distances (note the additional reciprocal lattice points in-between).

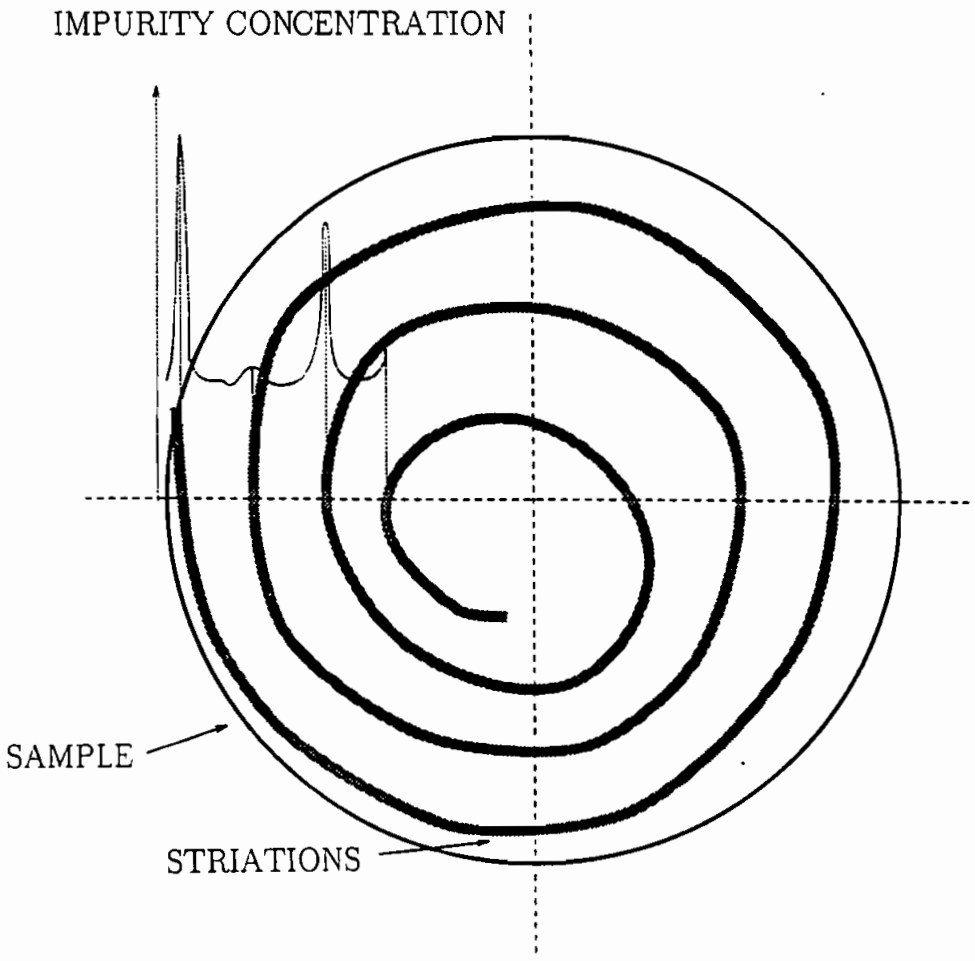

FIGURE 10 Linescan of RBS measurement along the radius of a section perpendicular to the growth direction of a Beryllium single crystal. Enhanced concentrations of iron and carbon coincide with striation line.

approximately 4.9% /21/ which should play an important role for the defect formation. From this point of view it should be important to control the temperature gradients in this temperature region. If different crystal growth techniques are compared concerning the local function of temperature variation a drastic difference can be found: (beside the already mentioned non radial temperature distribution along the cylinder perimeter). Due to the relatively small region where the light is focused the cooling process is very fast, taking minutes as compared to growth techniques like Bridgman or Gradient freeze where it may even last days. Considering the previously mentioned phase transition or frozen residual stresses drastic consequences for the real structure development can be supposed.

The first step in controlling the local temperature field is its characterization. For that reason measurements and some modelling of the thermal growth conditions

was undertaken /15/. Figure 11 shows the temperature course along the growth axis (fig. 11a) and the corresponding temperature gradient (fig. 11b), calculated in a one dimensional study. The intention to minimize the temperature gradient, in order to reduce the dislocation density formation during cooling, could be realized in a simple experiment by changes in the illumination geometry i.e. by a controlled defocusing of the lamps. This was carried out by an outward shift of up to 10mm of the lamps away from the focal positions in the elliptical mirrors. The result is a significant reduction of the maximum temperature gradient especially with a defocusing of 5mm (fig. 11b). On the other hand the temperature gradient at the solidification front became higher by this defocusing. It is known that higher temperature gradients at the solidification front reduce the supercooling effect.

A more sophisticated (three dimensional) model considers also the thermal convection in the vertical cylindrical configuration and allows the calculation in every vertical as well as radial distance /15/. Figure 12 shows the radial temperature distribution with the distance from the solidification front as a parameter. Due to the thermal convection an increasing curvature of temperature distribution with augmenting distance from the solidification front can be noted, which should be connected with a higher local lattice strain during the cooling process. Using the maximum radial temperature difference of 260 K, calculated 11.5 mm away from the solidification front (fig. 12), a maximum thermal stress of 890 MPa can be calculated, which must be removed by plastic flow and the creation of dislocations. Therefore the reduction of the maximum temperature gradient in the crystal during cooling should be important.

γ-ray Rocking curves in fig. 13a show the effect of the healing of weak subgrain boundaries by an annealing process, but in the case of higher misorientations (fig. 13b) the subgrain boundaries seem to be connected to stable arrangement of strain effective precipitates (comp. fig. 8) leading to blocking or even reformation of subgrain boundaries. Figure 13c represents regions of increased lattice perfection due to the manipulators leading to reduced temperature gradients during solidification. While the former growth process produces an intrinsic mosaicity of typically (3–6) minutes of arc (FWHM), reduced temperature gradients in azimuthal and longitudinal directions deliver partial volumina of (0.6–1.5)′ in FWHM.

The γ-ray diffraction with an energy of e.g. 662 keV is connected to very low Bragg angles of tenths of a degree. Due to typical beam dimensions of $(5 \times 1)\text{mm}^2$, it is difficult to make statements about homogeneity in bigger volumes, from this technique. Some information about the volume of the crystal can be collected more easily by topographic methods. Figures 14a and 14b/22/ show two different images of X-ray topography. The first one (fig. 14a) exhibits a rather homogeneous contrast of a plate cut along the growth axis with a very homogeneous volume parallel to the c-axis of the hexagonal lattice (growth direction). Figure 14b shows quite the opposite behavior of a non basal reflection from the whole volume of the same crystal. In the latter case the high residual stresses, which have been discussed above should also play an important role. Such residual stresses should be connected with radial macroscopic strain fields, which are well known to be M- or W-shaped as they are studied extensively in semiconductor crystals. These problems are still under investigation.

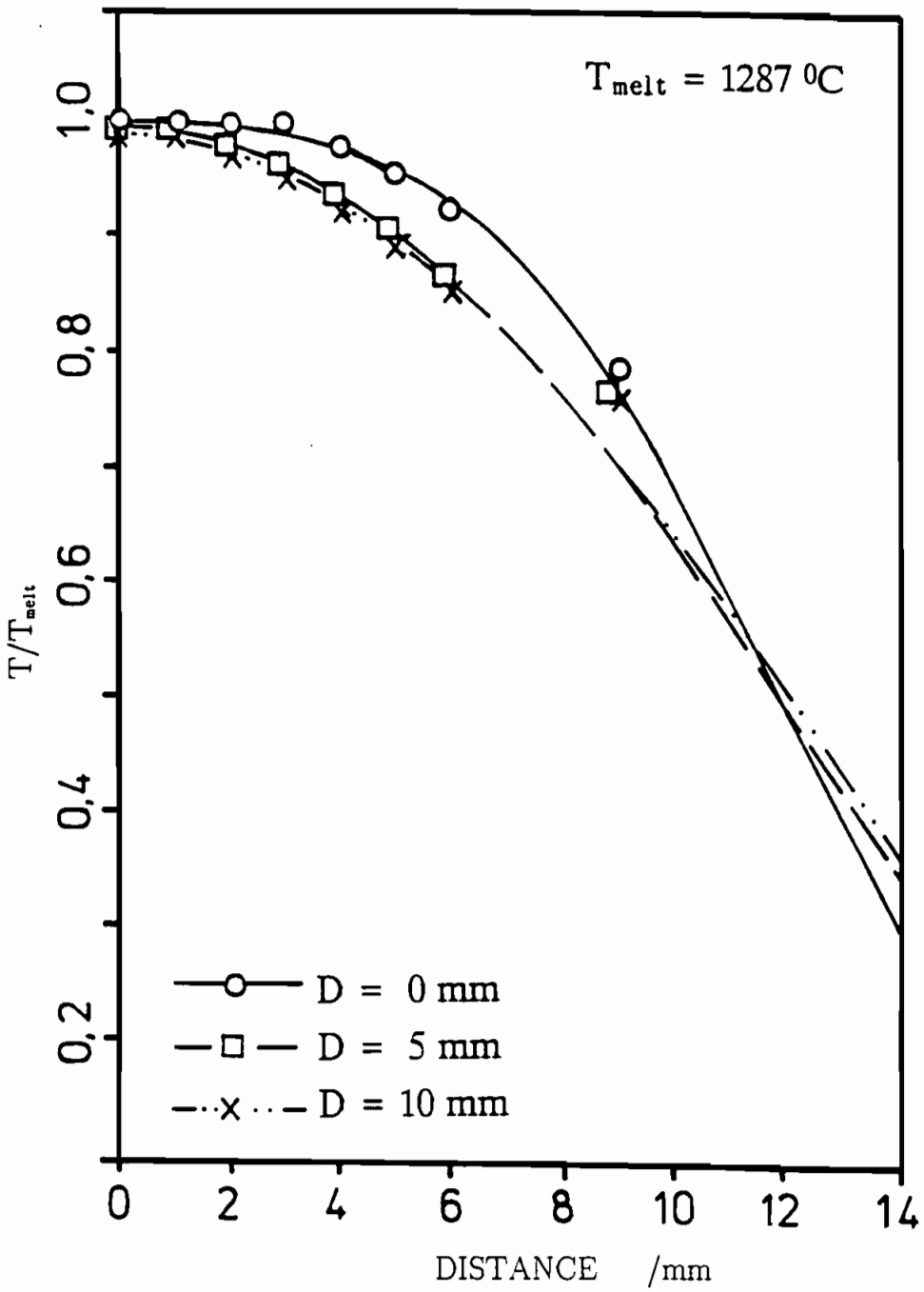

FIGURE 11 Distribution of temperature versus the vertical distance from solidification front. Symbols indicate points of measurement which are fitted well by an one-dimensional approach (a). (b) shows the temperature gradient versus vertical distance from the solidification front. The defocusing experiment /14/ clearly shows a reduction of maximum gradient but the phase transition (at 1523 K) is shifted to shorter distances from the solidification front.

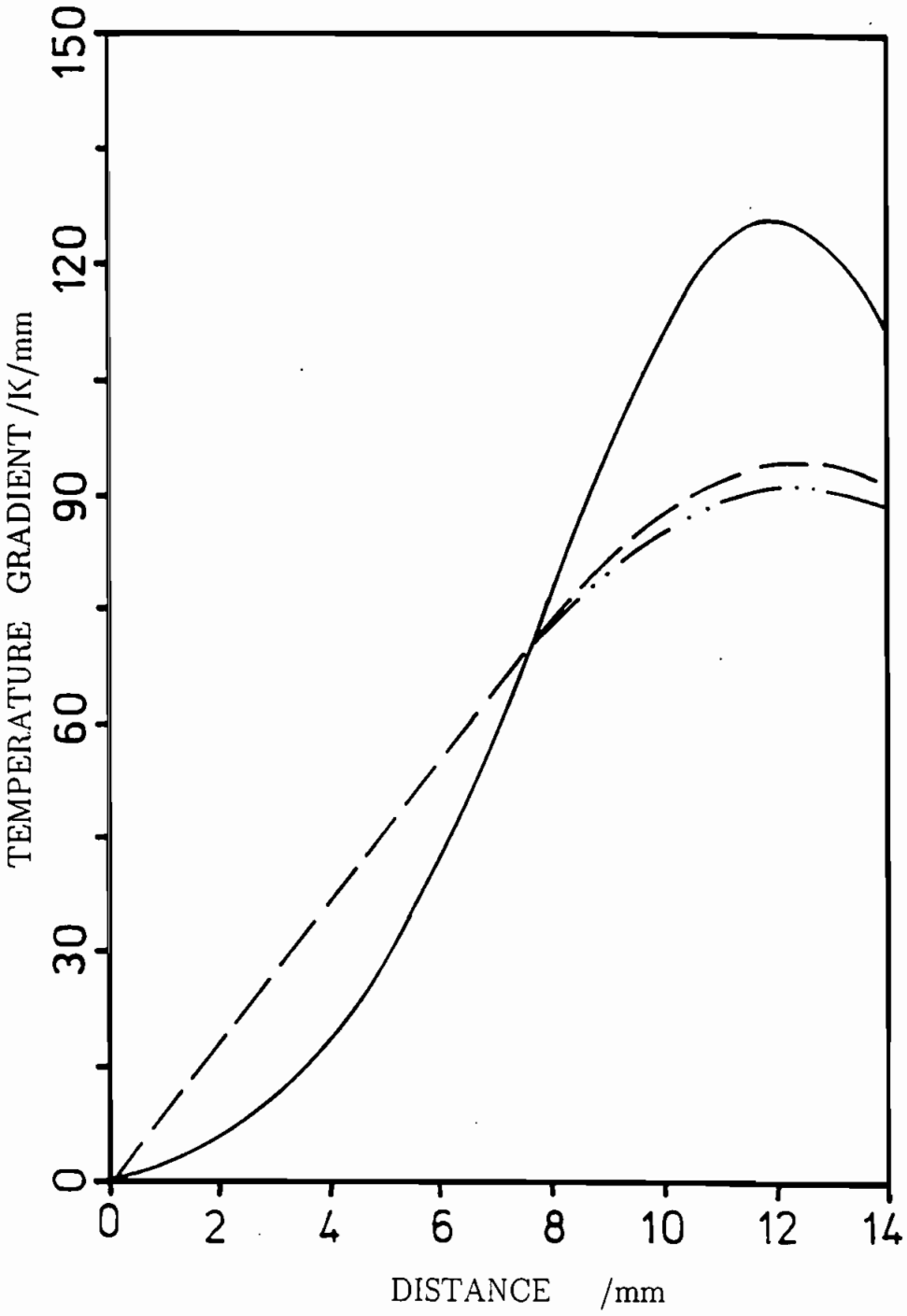

FIGURE 11 (*Continued*)

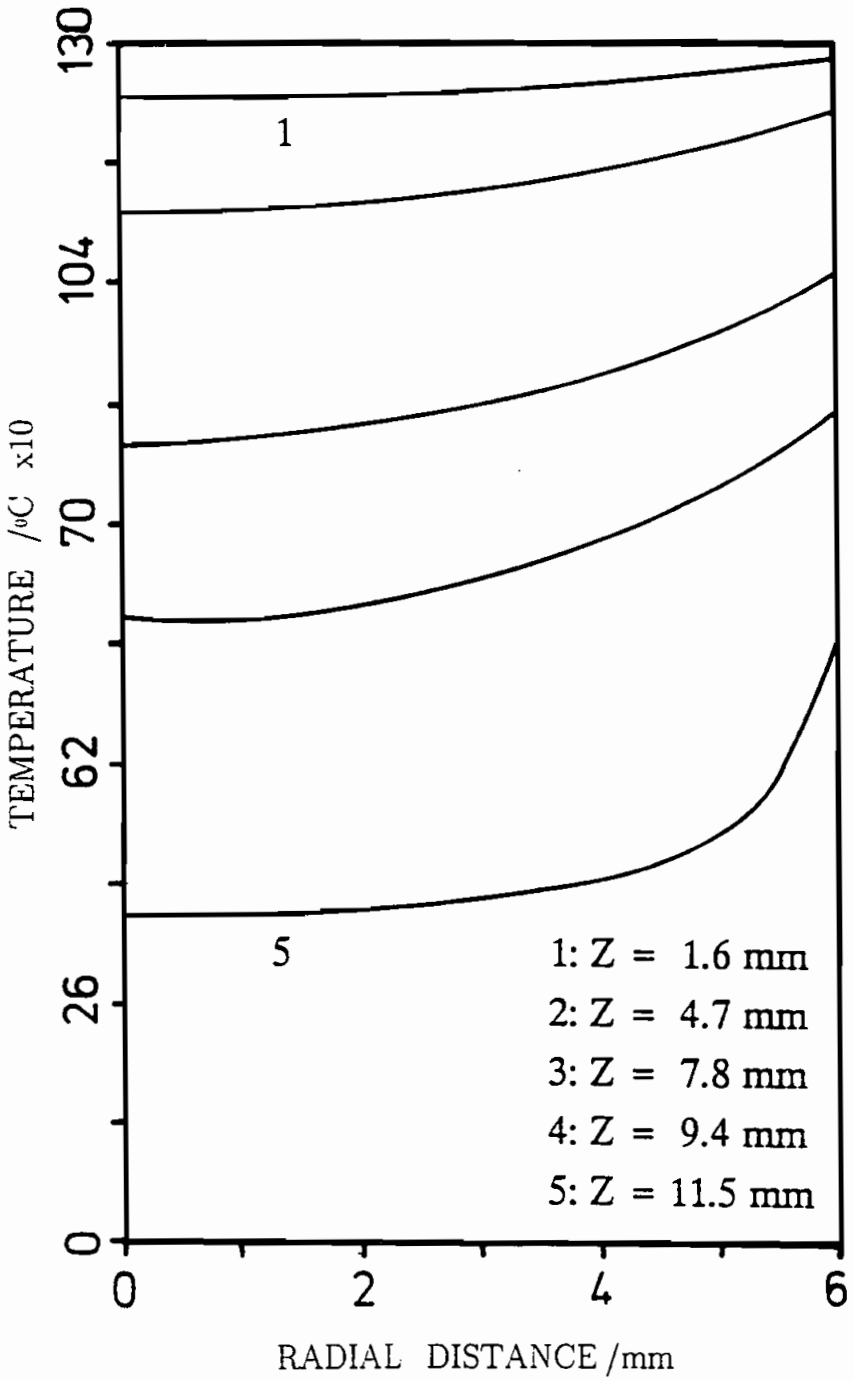

FIGURE 12 Temperature distribution versus radial distance from growth axis with the distance from solidification front as a parameter (see text).

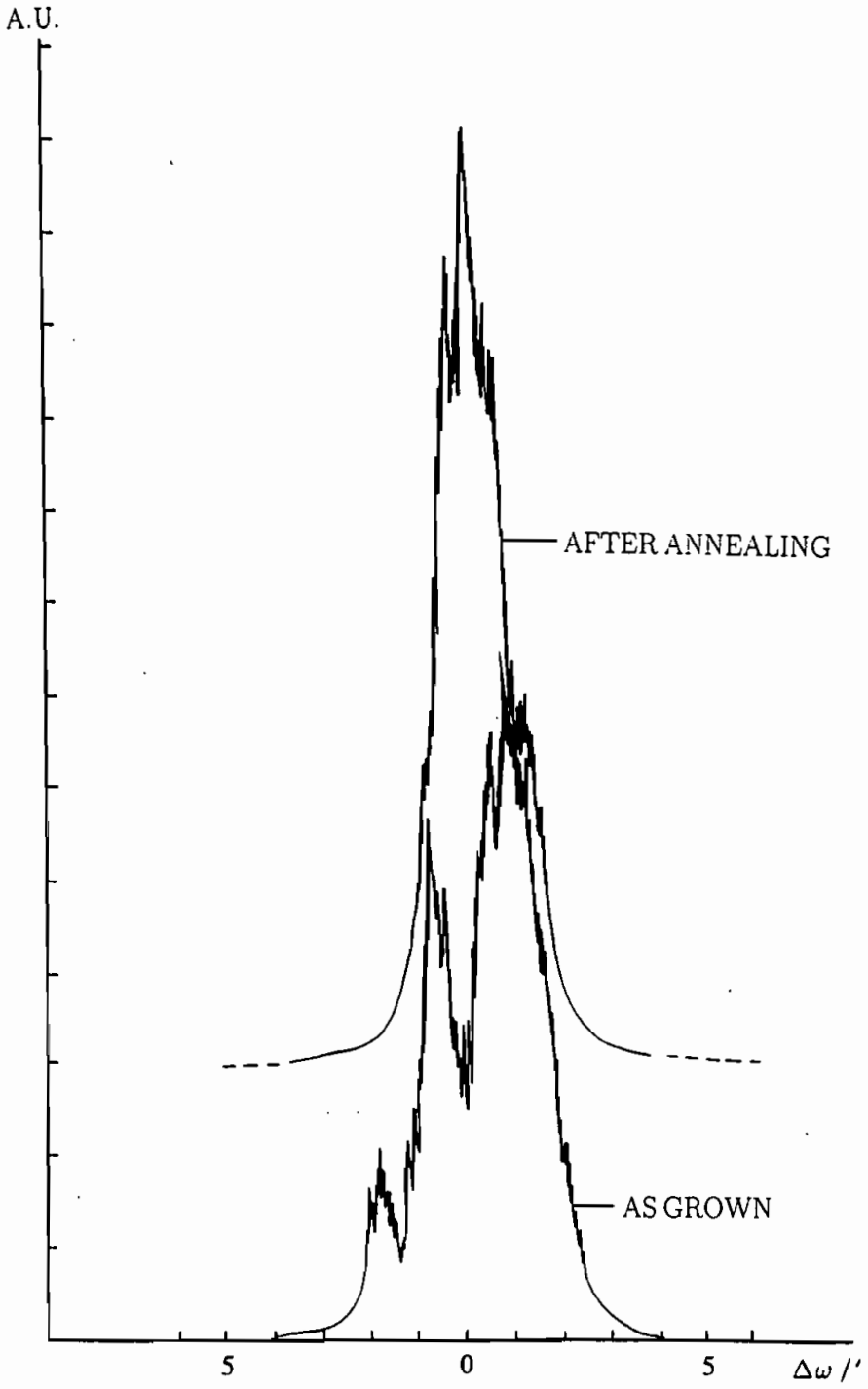

FIGURE 13 Influence of crystal lattice defects on rocking curves (662 keV γ-ray) by modifications in crystal growth and annealing processes. (a): healing effect of subgrain boundaries during a 1323 K annealing of 8 h compared with the as grown state. (b): In regions of higher impurity content of the same crystal, subgrain boundaries seem to be stabilized by precipitation arrangements (comp. fig. 8). (c): higher perfect region due to homogenization and reduction of temperature gradient by defocusing.

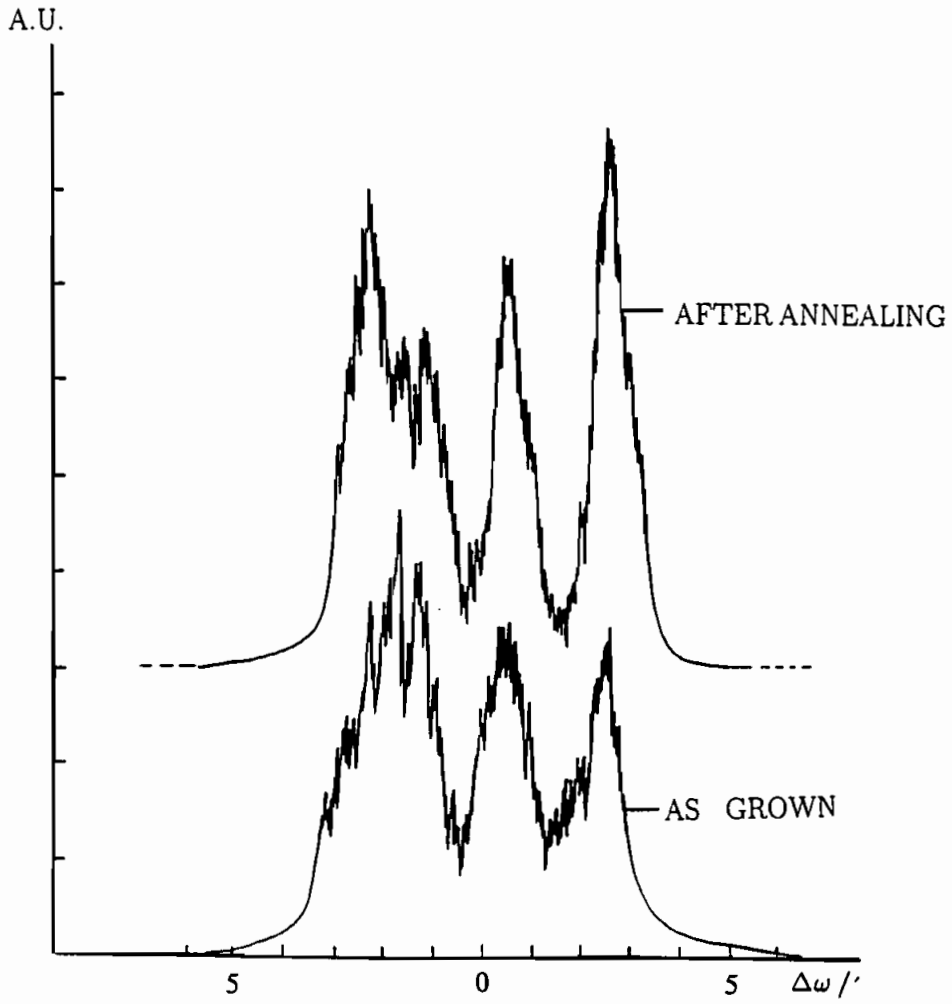

FIGURE 13 (*Continued*)

APPLICATION OF AS GROWN CRYSTALS AS SYNCHROTRON MONOCHROMATORS

The application of Beryllium as an advanced monochromator material also for synchrotron radiation is the consequence of its exciting physical properties (see above). The increased brilliance with extremely low divergence of the synchrotron beam open up the possibility of completely new experiments in many different fields. As well as this, optical elements such as monochromators now have to fulfill much more stringent requirements. Depending on the proposed experiment Beryllium single crystals should have an intrinsic mosaic spread below 1′ or even around 30″ /4/. One of the most attractive of these applications is the multi beam

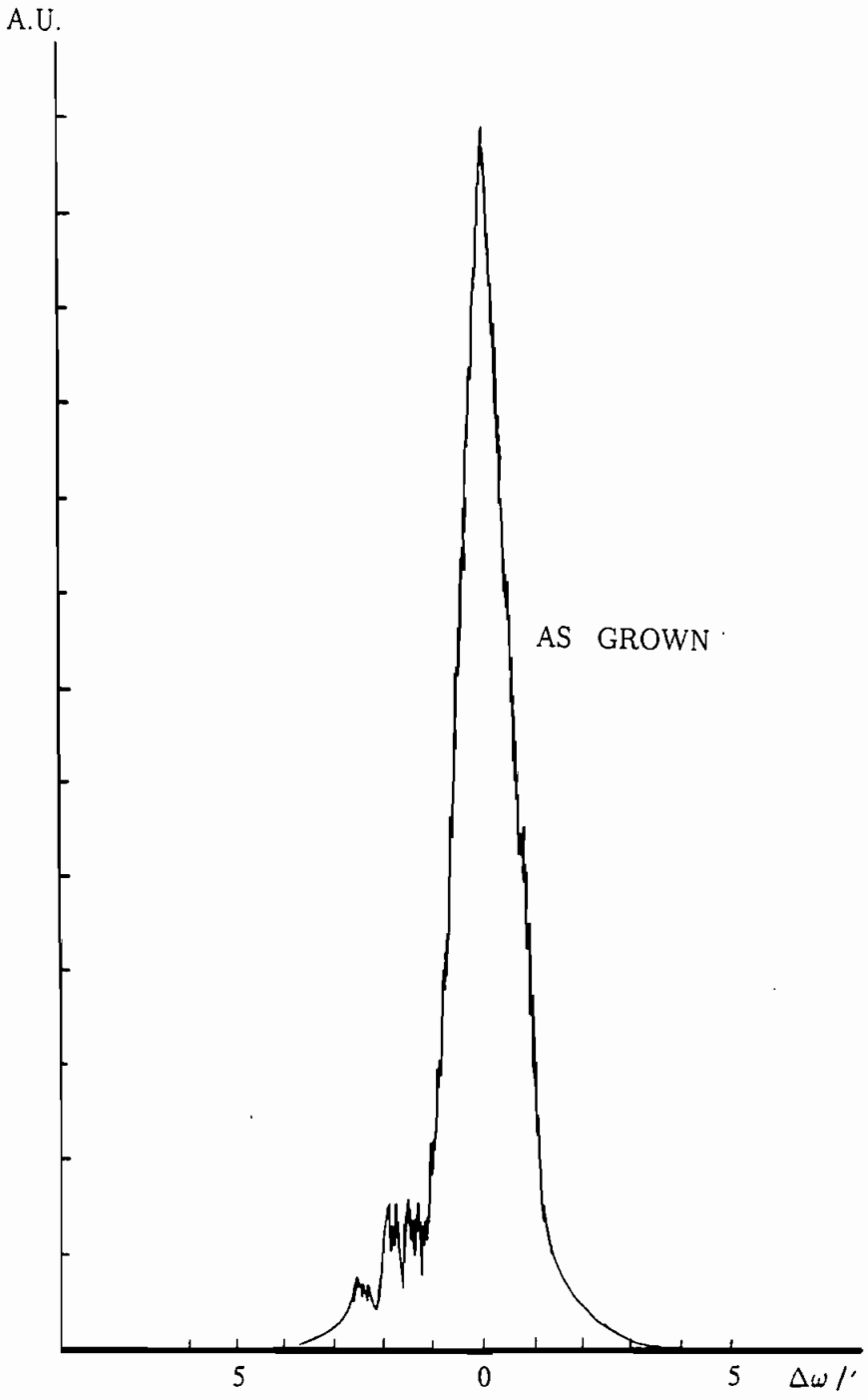

FIGURE 13 (*Continued*)

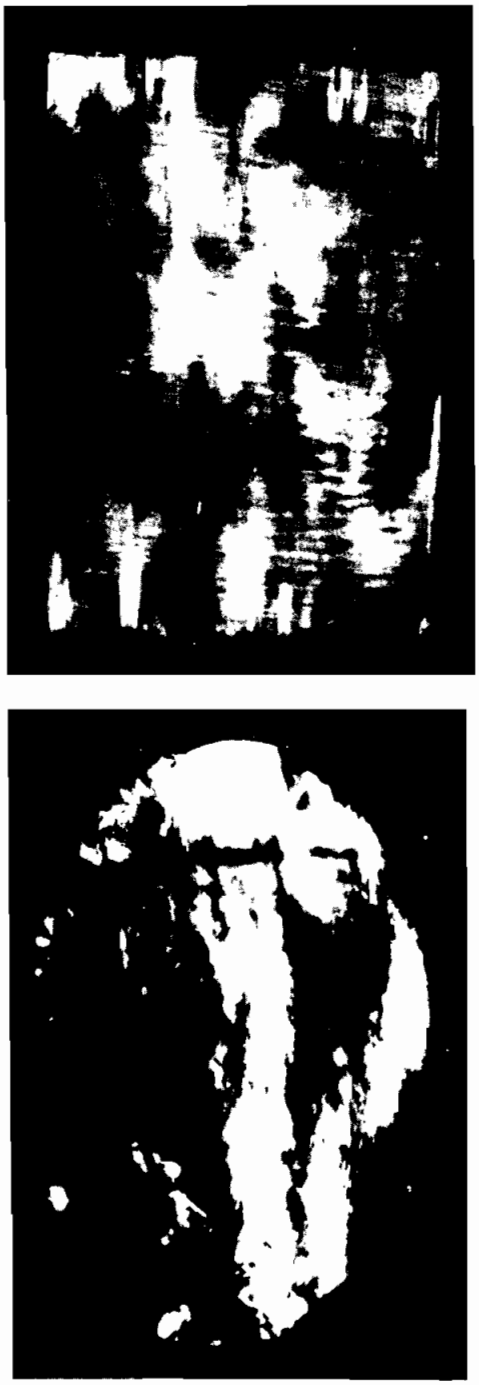

FIGURE 14 X-ray topography of as grown state. (a) indicates a rather perfect crystal lattice by a homogeneous reflection intensity in a plate cut along the growth axis parallel to the c-axis of the hexagonal lattice. (b) exhibits an inhomogeneous volume of an oblique part of the same crystal.

utilization /23/. The highly intense polychromatic beam of an undulator source penetrates the single crystalline Beryllium slice. In spite of a strong heat load of up to 18 W/mm^2, the especially low absorption and highly effective cooling (high thermal conductivity and capacity) leads to a relatively low heating up of only a few degrees whereas conventional materials like Silicon would be molten immediately /24, 4/. Due to a high Youngs modulus the lattice deformations produced by thermal gradients are low. Using a perpendicular orientation of the basal planes with respect to the surface, the Beryllium slice acts as a Laue monochromator and reflects the chosen wavelength out of the beam and to the experimental set-up. The intensity of the reflected beam can be controlled by the crystal thickness. The transmitted spectrum has now lost this wavelength but following Beryllium crystals may reflect other wavelengths of the spectrum. In consequence a single synchrotron beam of the facility can be exploited several times with little loss in intensity and quality. The special high heat load stability allows fluxes up to four orders of magnitude higher than conventional silicon crystals /23/. Another application will use the same idea for precise position control of the synchrotron beam around the whole storage ring facility in connection with position sensitive detectors. Finally, besides the thermal peculiarities, the previously mentioned low lattice distances lead to high Bragg angles even for higher energetic beams. Thus better resolution functions allow the construction of double crystal monochromators with the highest resolution also in this region of wavelengths /11/.

CONTROL OF INTRINSIC MOSAICITY BY DEFORMATION PROCEDURES

All the different applications demand single crystal materials with different defect concentrations and defect structure distributions respectively. Thus, for chosen reflections (lattice distances) the special scattering behavior concerning intrinsic mosaicity in different directions, reflectivities, intensity ratios of different harmonics etc. are manipulated. For Beryllium crystals we are just at the very beginning of the development of such made-to-measure materials. Nevertheless todays knowledge should be discussed.

It has been mentioned that the group of potential neutron applications needs higher defect densities in homogeneous distributions. Intrinsic mosaic spreads should come up to (20–40)′ due to relatively high divergencies and the limited flux of neutron reactors.

Common techniques to increase the mosaicities of single crystals with more or less isotropic lattices such as Copper only require relatively simple deformation steps to incorporate appropriate dislocation densities /8/. Analogous experiments in Beryllium to widen the (0002) mosaicity had not been very successful. To explain this some of its mechanical individualities should be recalled.

Unlike Copper, the deformation behavior of hexagonal Beryllium is extremely anisotropic /25/. It can be seen from the critical resolved shear stresses (CRSS) versus temperature diagram (fig. 15) that plastic deformation behavior for different slip systems exhibits different temperature dependencies. There is also a strong dependence on the local impurity content /25/.

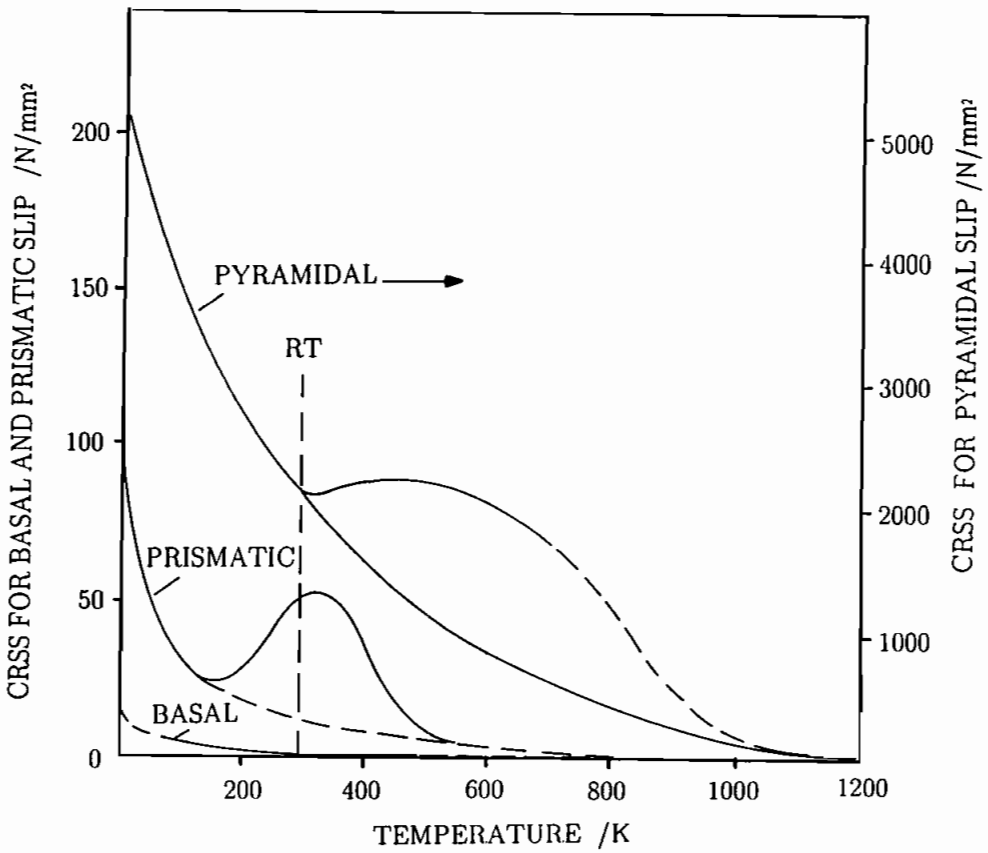

FIGURE 15 Critical resolved shear stresses (CRSS) versus temperature for different slip systems. At room temperature the ratio of basal:prismatical:pyramidal slip is known to be approximately 1:40:2000 MPa /25/.

One of the most interesting reflections to be influenced in its mosaicity is the strong (0002) basal reflection. In this case the problem of the broadening of the rocking curve is as follows:

Due to the anisotropic slip behavior of this lattice, basal and prismatic slips of the first order are normally the only slip that occurs. Table I indicates that for hexagonal metals the Burgers vectors in these slip systems always lie in the basal plane with the exception of prismatic slip of second order which has not been observed in Beryllium. Broadening of a reflection e.g. in an ω-scan, means the widening of the corresponding reciprocal lattice point perpendicular to the surface of the Ewald-sphere. This widening is a consequence of local bending of the real lattice by undulated or "roughened" lattice planes or, in the model of mosaic crystal, individual perfect mosaic blocks with a limited orientation distribution. These strain effects can be achieved in different amounts by the resulting strain fields around lattice defects such as point defects or defects of 1-, 2- or 3-dimensional types. Dislocations play the most important role due to their long range strain field. The

relation of their strain field and the scattering conditions are responsible for the dislocation contrast which is a common tool for dislocation characterization e.g. in topographic or microscopic techniques. In these terms the projection of the scattering vector **g** onto the Burgers vector **b** determines the intensity effect around the dislocation. If this projection is zero, i.e. if both vectors are perpendicular ($\mathbf{g} \cdot \mathbf{b} = 0$) the intensity effect should become a minimum for edge dislocations or even zero for screw dislocations. Therefore, a significant widening of the basal reflection needs Burgers vectors outside the basal plane which seem to be obtainable only by pyramidal slip (Table I).

Another way of generation of non-basal Burgers vectors in hexagonal metals might be the dissociation of dislocations e.g.:

$$\frac{1}{3}\langle 11\bar{2}0\rangle \leftrightarrow \frac{1}{6}\langle 11\bar{2}1\rangle + \frac{1}{6}\langle 11\bar{2}\bar{1}\rangle$$

Such dissociations represent the formation of stacking faults but they have not been observed in Be because of its high stacking fault energy /25/. Other "useful" defects had been reported in the literature as a spin off from creep tests at elevated temperatures /26/. Appropriate dislocation reactions at jogs and junctions respectively lead to the formation of dislocation loops with Burgers vectors perpendicular to the basal plane. Such loops have also been observed after irradiation with highly energetic neutrons up to doses of 8 dpa at temperatures of 623–673 K /27/.

Compression tests have been performed perpendicular to the c-axis to use prismatic slip at elevated temperatures of 463K. Due to its strong lattice distortion effect which would take most of the scattering volume out of the Bragg position this "high temperature" step had been combined with a preliminary "low temperature" step at 170 K up to 100 MPa /28/. The reason for this was to initially produce a lattice stabilization against torsion around the compression axis in this well known valley of CRSS around 170 K, and secondly to incorporate high densities of dislocations on prismatic lattice planes as a precondition for appropriate dislocation reactions at higher temperatures. The prediction was to produce high densities of c-type loops like in creep tests. Detailed explanations will be given in

TABLE I
Typical slip systems in hexagonal metals for basal, prismatic and pyramidal slip /25/.

	Slip system			Dislocation	
Name	Symbol	Slip plane	Slip direction	Symbol	Burgers vector
Basal	B	(0001)	$\langle 11\bar{2}0\rangle$	a	$\frac{1}{3}\langle 11\bar{2}0\rangle$
Prismatic					
First order	P	$\{10\bar{1}0\}$	$\langle 11\bar{2}0\rangle$	a	$\frac{1}{3}\langle 11\bar{2}0\rangle$
Second order	P_2	$\{11\bar{2}0\}$	[0001]	c	[0001]
Pyramidal					
First order	τ_1	$\{10\bar{1}1\}$	$\langle 11\bar{2}0\rangle$	a	$\frac{1}{3}\langle 11\bar{2}0\rangle$
			$\langle 11\bar{2}3\rangle$	$c + a$	$\frac{1}{3}\langle 11\bar{2}3\rangle$
Second order	π_2	$\{11\bar{2}2\}$	$\langle 11\bar{2}3\rangle$	$c + a$	$\frac{1}{3}\langle 11\bar{2}3\rangle$

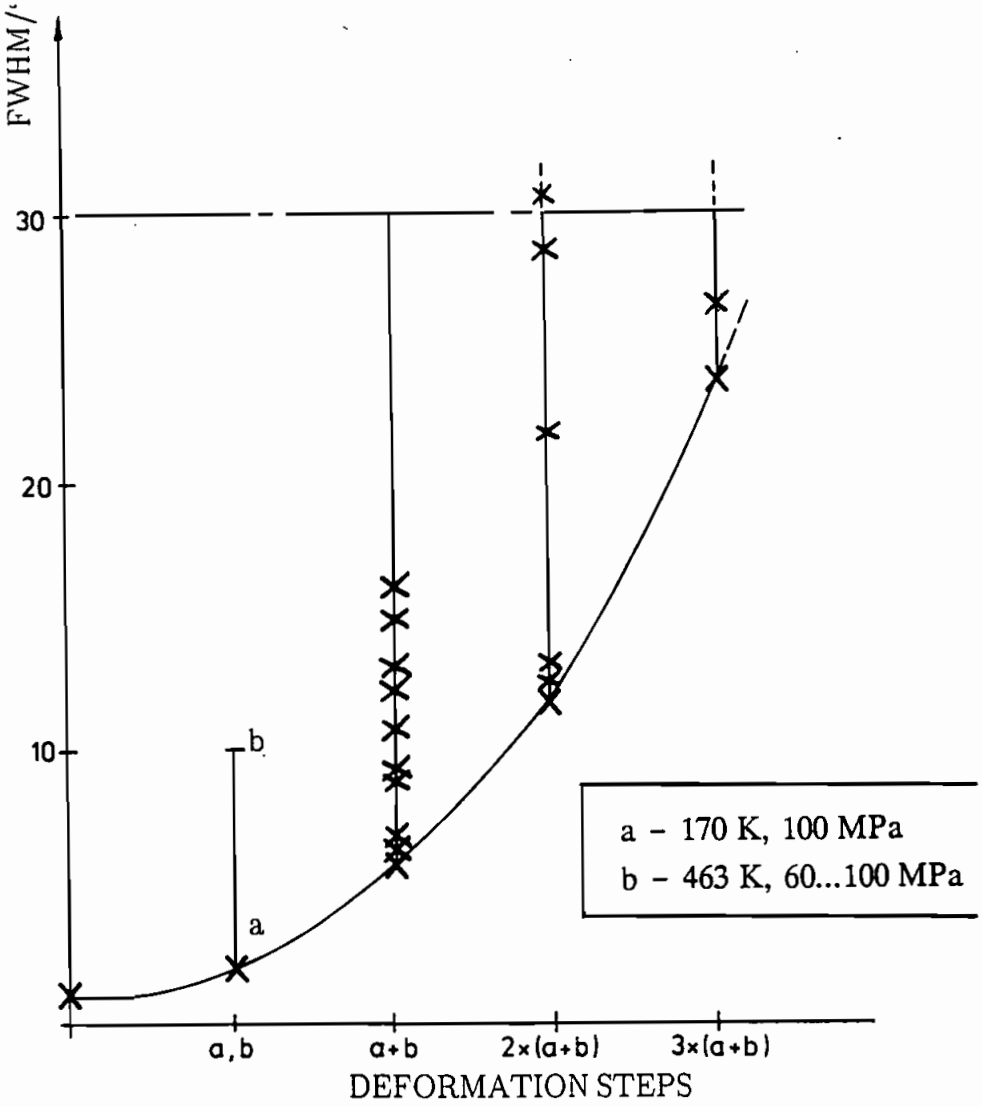

FIGURE 16a Influence of different deformation stages on mosaic spread, measured by γ-ray diffraction. The "high temperature" step (b) simulates a stronger widening of mosaic spread due to effects of lattice torsion, while the combination of both steps really leads to the desired effect. Repetition of the whole cycle allows the adjustment of final mosaic spread.

/28/. Figure 16a presents the influence of these treatments on the intrinsic mosaicity. Repetition of the multistage deformation enables the adjustment of the desired value /29/. Figure 16b presents the accompanying rocking curves which in the ideal case should represent a Gaussian distribution of the individual mosaic blocks.

What are the reasons for these different effects on the mosaic spread in (0002) at low and elevated temperatures, since no indication of pyramidal slip could be

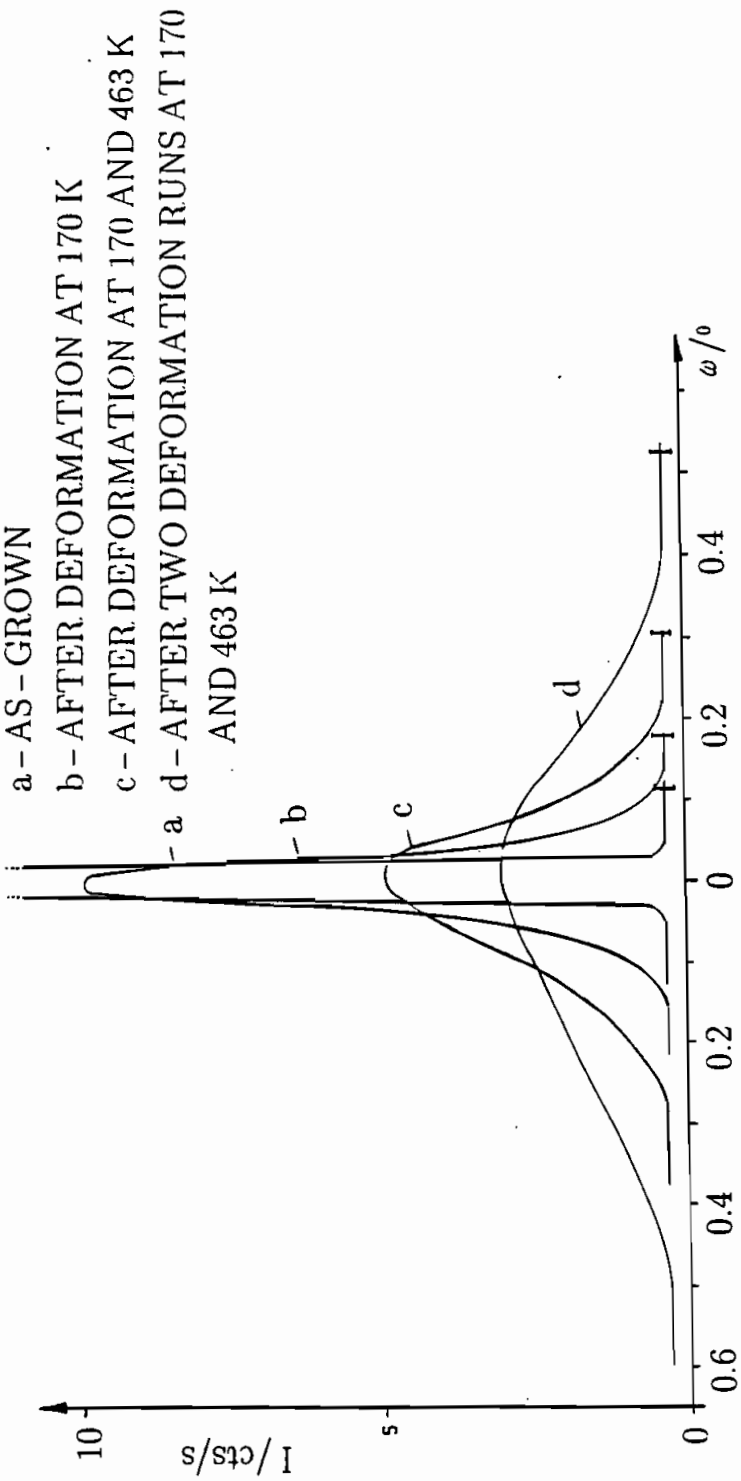

FIGURE 16b γ-ray rocking curves after different steps of deformation.

FIGURE 17a TEM-image (1000 kV) of c-type Loops in the deformed samples after pinning with He-ions /28/.

found? Firstly, the low temperature deformation should lead to strain hardening in consequence of dislocation multiplication and migration with "classical" Burgers vectors lying in the basal plane. Therefore, no significant broadening of basal reflections is observed. Secondly the compression at elevated temperatures leads to dislocation reactions generating point defects of vacancies and interstitials, coagulating to dislocation loops with Burgers vectors in the <0001> direction. These loops should be responsible for the considerable widening of the orientation distribution of the mosaic blocks.

The TEM-characterization of these predicted loops was successful only after their blocking against slip in the basal plane. For this reason the TEM samples had been irradiated, before final thinning, with He-Ions of 3 MeV to a displacement rate of 0.5 dpa. Figure 17a reveals a typical loop concentration in deformed samples with broad mosaicities. They consist of an agglomeration of atoms situated on interstitial sites on the basal plane. The Burgers vectors of the surrounding dislocation is of the 1/2<0001> type and results in bending of the adjacent basal planes. Energetic aspects should lead to stacking faults above and below such loops in hexagonal metals (fig. 17b) but no indications of stacking faults have been found so far /28/. On the other hand perfect loops with Burgers vectors [0001] are also

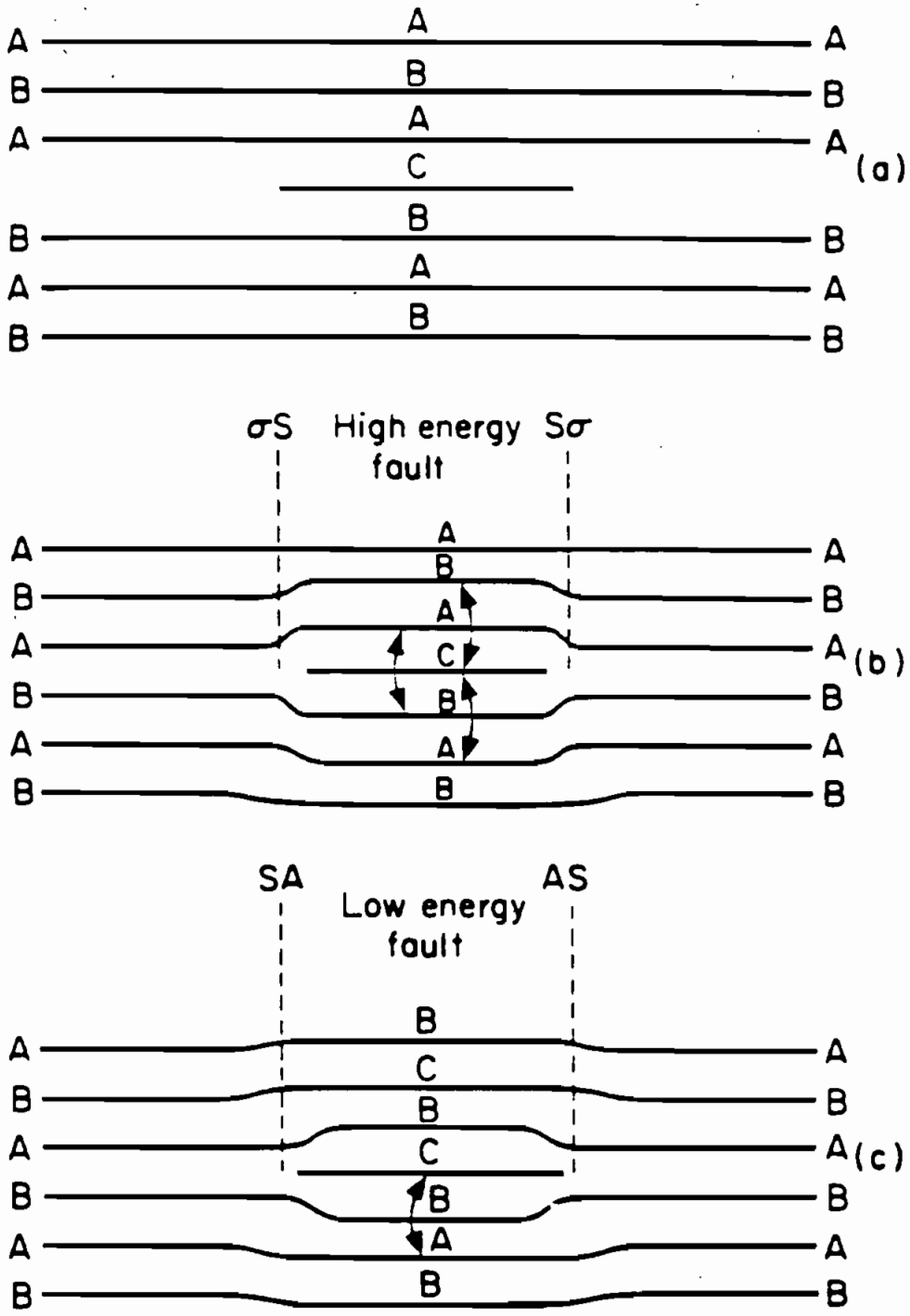

FIGURE 17b (a) Precipitation of a layer of interstitials. (b) Prismatic loop resulting from the layer of interstitials; the loop contains a high-energy stacking fault. (c) Prismatic loop containing low-energy stacking fault. Burgers vectors should be ½ [0001], but perfect loops with Burgers vectors [0001] are also observed in irradiated Cadmium and Zinc /30/.

observed in irradiated Cadmium and Zinc. They result from double layers of interstitials /30/.

CHARACTERIZATION OF NEUTRON SCATTERING BEHAVIOR

The discussion of neutron scattering behavior will be focused mainly on some of the intensity aspects in connection with the unusual properties of Beryllium.

Measurements of the neutron reflection intensities with different FWHM in mosaicity indicates several further influences which are responsible for deviations from the maximum expected peak reflectivities.

Figure 18 shows the typical reflection and transmission behavior of a deformed Beryllium sample in a rocking experiment with thermal neutrons at wavelength of 0.2 nm. On the one hand the reflection curve does not touch the upper limit of primary intensity as might be expected from the high coherent cross section and low absorption. On the other hand, the transmission curve does not come down to zero at the optimum Bragg position although the thickness of the sample is higher than the theoretical reflection depth. The transmission curves are lower than the primary intensity also outside of angle range of reflection curve. The reason for that behavior can be connected with the deviations from the already mentioned model of an ideal mosaic crystal and the occurrence of extinction processes such as are known from extensive investigations of Copper crystals /8, 10, 31, 32, 6, 7 2/. An influence which has to be considered even if homogeneous mosaic distribution functions could be achieved is the probability of additional (parasitic) reciprocal lattice points touching the Ewald sphere. Figure 19 illustrates the main aspects of these influences. First of all the low lattice distances in Beryllium implies a low density of reciprocal lattice points in the reciprocal space. This is an additional advantage of this material compared to conventional ones such as Copper. Depending on the azimuthal position (ψ) of the lattice around the scattering vector additional lattice points besides **hkl** may touch the Ewald sphere and "drain off" intensity in corresponding directions (parasitic reflections or Umweganregung). Obviously the probability for that behavior increases with shorter wavelengths, higher divergences and also broader smeared lattice points, i.e. larger broadened mosaicities. This also emhasizes the importance of the azimuthal scattering position for these disturbing effects which lead to intensity losses in the desired reflection /28/. Figure 20 presents a map of additional reflections in dependence of the wavelength of neutrons and the azimuthal lattice position (ψ) around the scattering vector, calculated using the basal reflection as the primary one. Only in regions away from the trace curves can unreduced primary reflection intensities be expected. Beam divergence is not considered and would widen the curves considerably. Therefore in lower regions of short wavelengths undisturbed primary reflection would be rarely, if ever, expected. Corresponding measurements confirm this idea /28/. Consequently this problem may be discussed in connection with favorable azimuthal lattice positions, minimum intensity loss in the primary reflection, minimum useful wavelength and maximum desirable mosaicity.

The rest of the intensity of transmitted neutrons indicates that there is still a non-optimal defect distribution in the lattice. Figure 21 presents neutron mea-

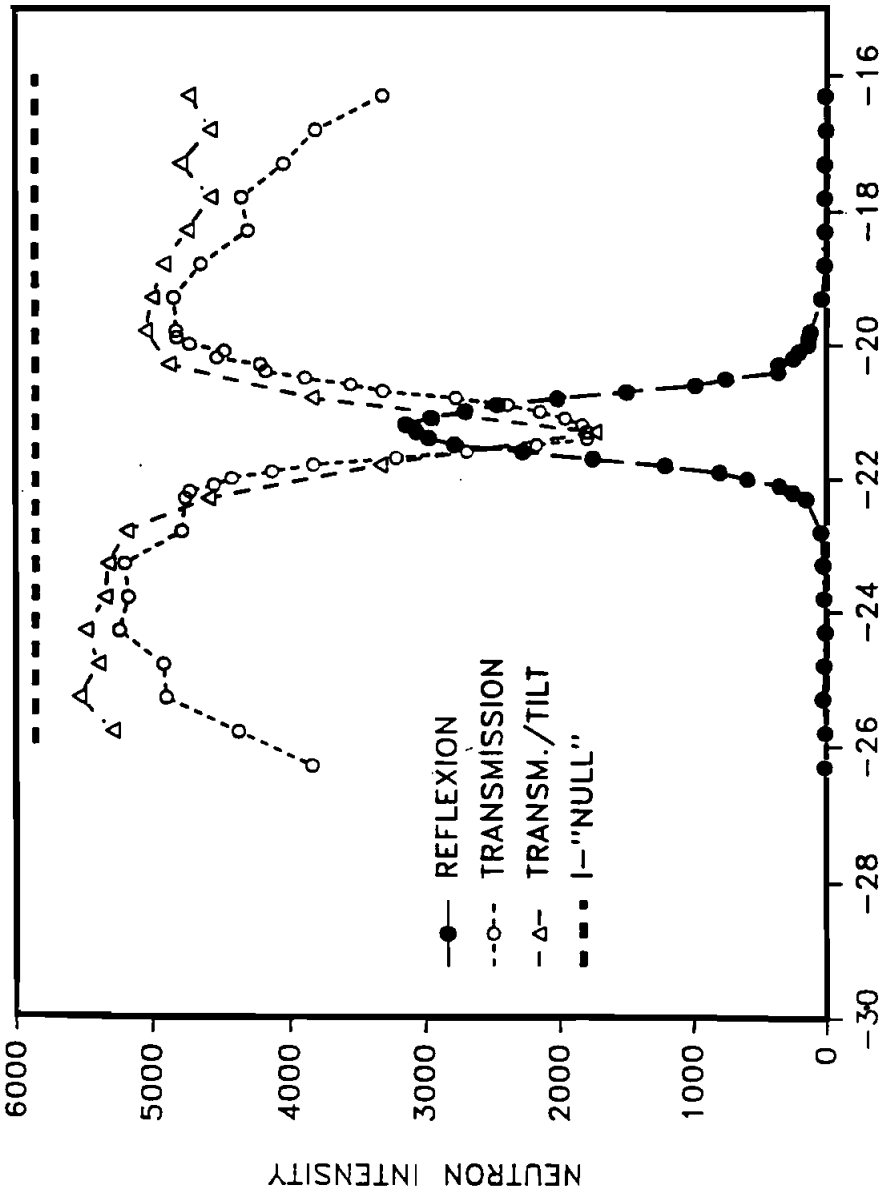

FIGURE 18 Typical reflection and transmission curves of a rocking experiment of (0002) reflection with neutrons.

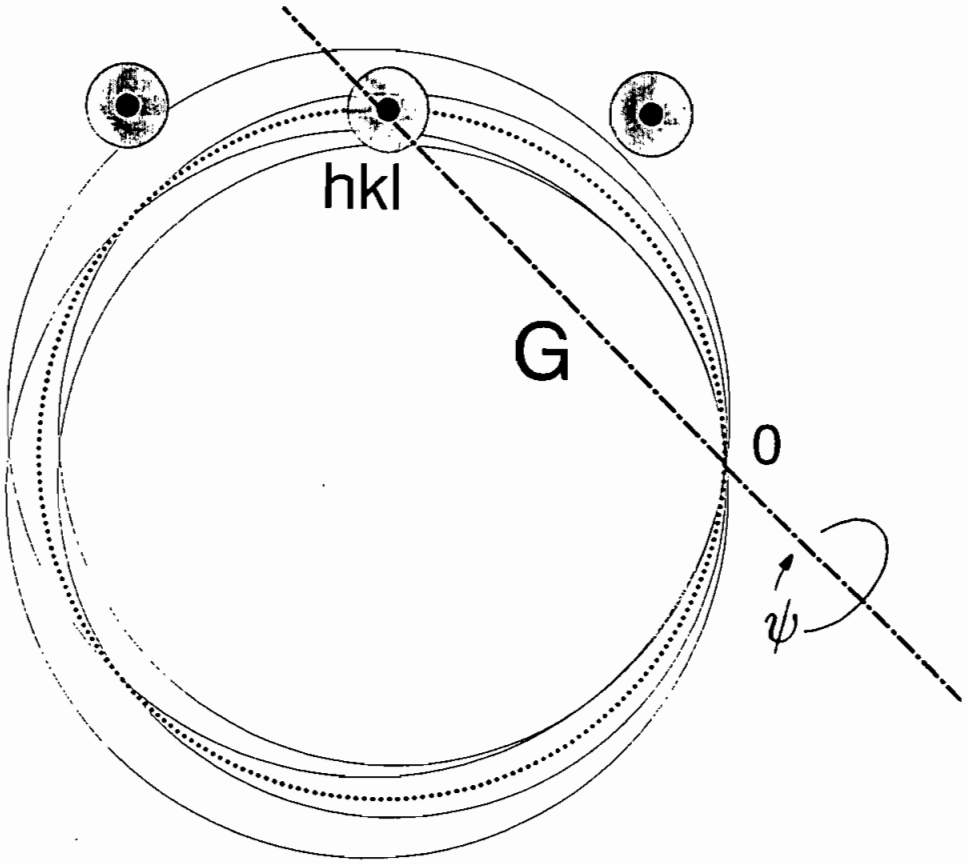

FIGURE 19 Illustration of occurrence of additional lattice points in consequence of smeared reciprocal lattice points and increased divergence of primary reflection (see text).

surements of a prismatic reflection and the corresponding transmitted beam in an as grown crystal plate. Azimuthal rotations of the sample around the scattering vector changes the transmitted intensity drastically and demonstrates the intensity loss by this mechanism. The comparison of different sample positions (second curve) proves the negligible influence of local inhomogeneities. Though the "certainty" of the as grown reciprocal lattice points is high, this experiment emphasizes the anisotropy of defect structure, which is frozen in already during crystal growth. Figure 22 show the significant reduction of this anisotropy by an annealing process. Note the significant raising of the transmitted intensity which indicates a lower probability of additional reciprocal lattice points on the Ewald-sphere, or reduced dimensions of the individual reciprocal lattice point (comp. fig. 19). The anisotropy of the as grown state is strongly enhanced by uniaxial plastic deformation, but moreover it is suggested that the three-dimensional stress distribution in the macroscopic sample also leads to a local inhomogeneous plastic flow in the basal plane, even if it has been oriented precisely perpendicular to loading direction. Therefore

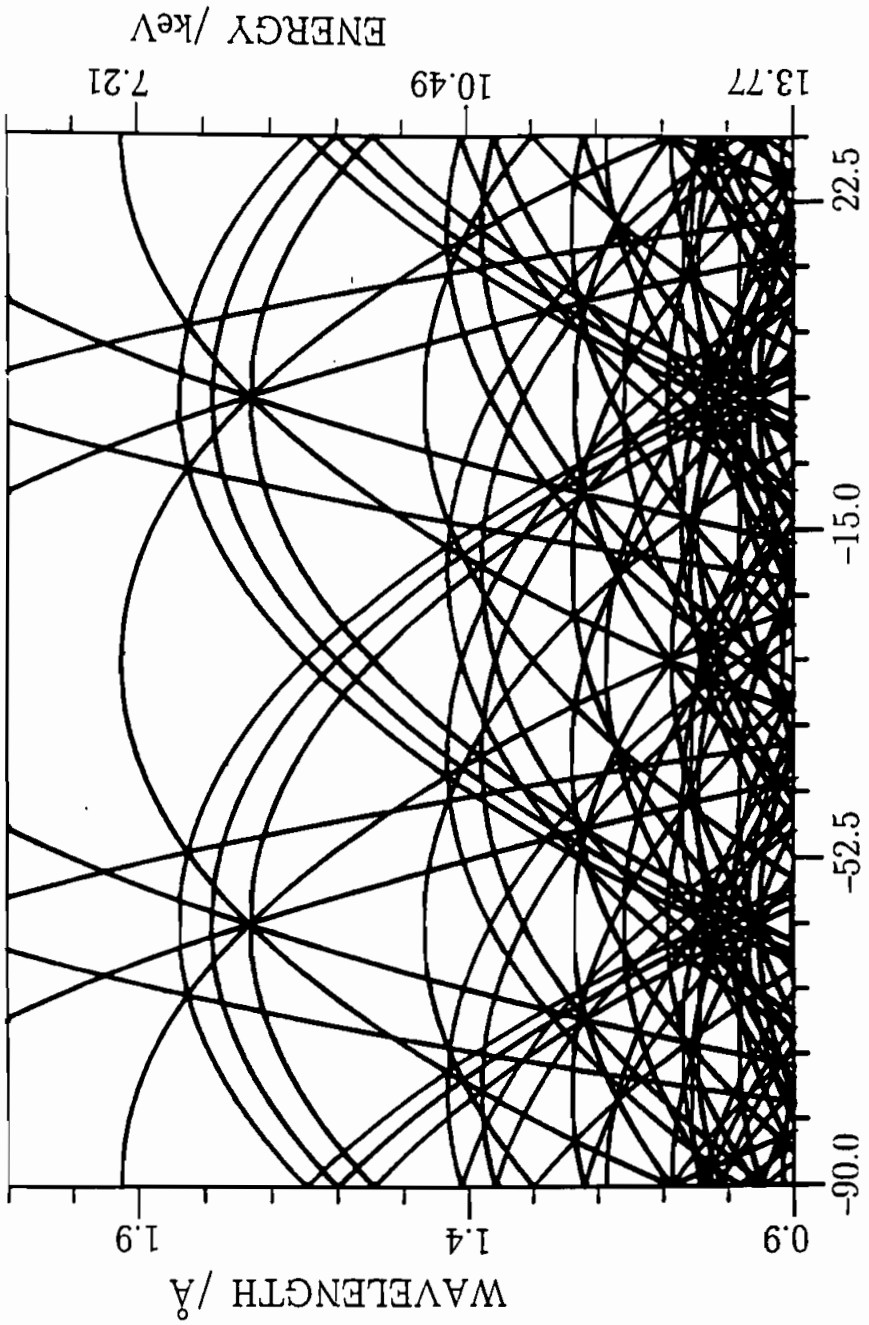

FIGURE 20 Calculated map of additional reflections in dependence of the wavelength of neutrons and the azimuthal lattice position (ψ) around the scattering vector. Only in regions away from the trace curves can unreduced primary reflection intensities occur. Beam divergence is not considered and would widen the curves additionally. Therefore in lower regions of short wavelengths undisturbed primary reflection would be rare or even impossible /14/.

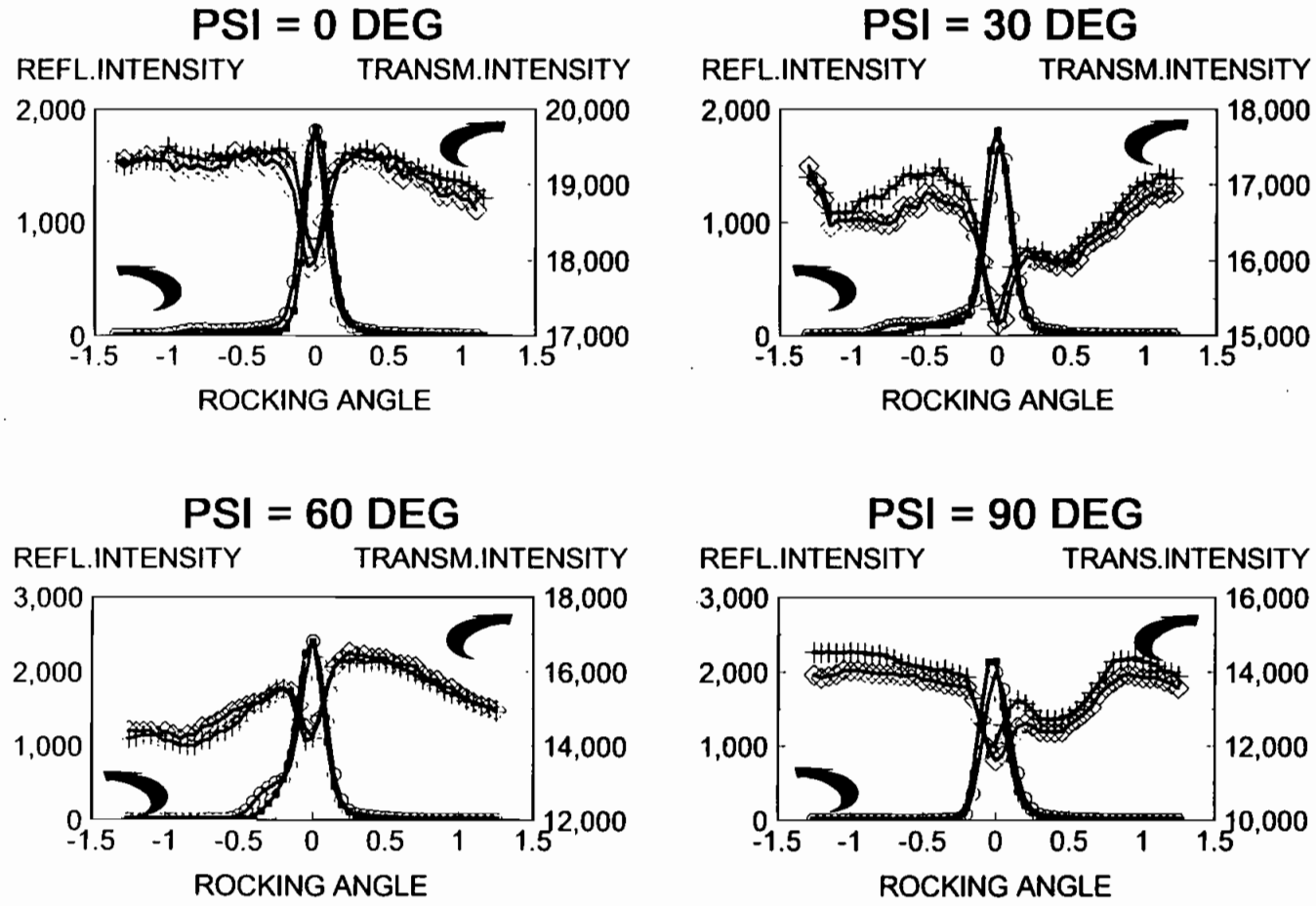

FIGURE 21 Neutron measurements of reflected and transmitted intensity ($20\bar{2}0$) of an as grown crystal plate in different azimuthal positions ψ (rotated around the scattering vector). The transmitted beam clearly indicates the intensity loss due to additional (parasitic) reflections. Two curves show the negligible influence of local inhomogeneity of the crystal.

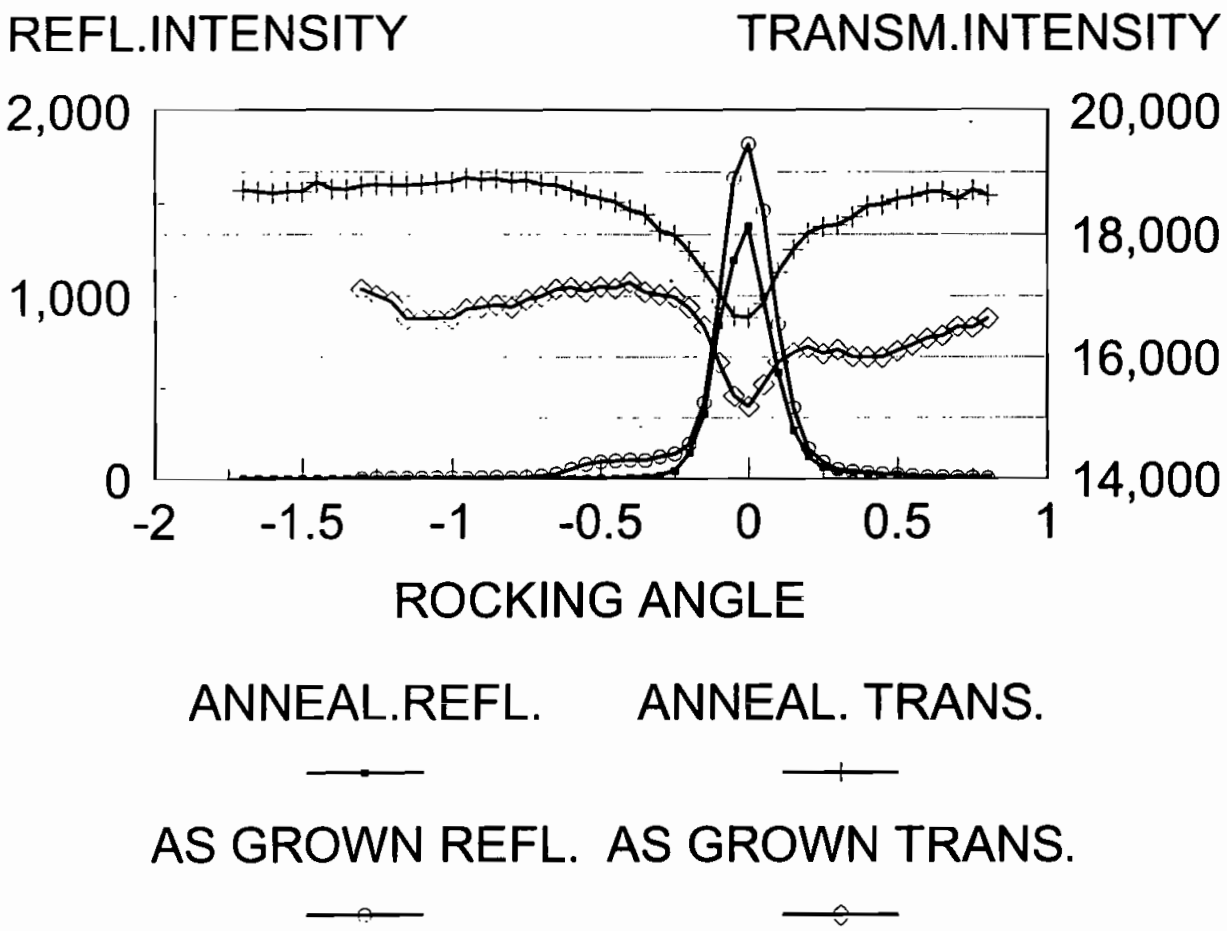

FIGURE 22 Example of "Purification" of transmitted intensity of $(20\bar{2}0)$ by an annealing process. Note the signficant raising of transmitted intensity in comparison to the as grown one. The dimensions of the individual reciprocal lattice points are reduced as well as the probability of additional (parasitic) reflections. The transmitted beam reaches a stable upper level.

possibilities of reducing the strong anisotropy of CRSS in the single crystal state should be investigated.

CONCLUSIONS

In the potential applications of X-ray monochromatization, particularly that of modern synchrotron facilities as well as in monochromatization of neutrons, different materials based on Beryllium may offer substantial progress. Their realization demands a real control, not only of mosaic spread but of the whole local defect distribution function and its anisotropy, and calls for theoretical and experimental investigations and developments of this material. By this means single crystal Beryllium materials offer unique potential if they can be developed from a metal, with initially exciting but rather noninfluencable properties, up to a made-to-measure advanced material.

References

1. M. S. Lehmann, J. R. Schneider, *Acta Cryst.*, **A33**, 789 (1977).
2. B. Dorner, *J. Appl. Cryst.*, **4**, 4, 185 (1971).
3. A.K. Freund, 5th National Conference on Synchrotron Radiation Instrumentation, Madison, Wisconsin, June 1987, (1987).
4. A. K. Freund, Proc. SPIE Conf. Nr. 1740, July 1992, San Diego, (1992).
5. M. v. Laue, X-ray Interferences (Akademische Verlagsgesellschaft, Leipzig, 1941).
6. J. R. Schneider, *J. Appl. Cryst.*, **8**, 195 (1975).
7. M. Kuriyama, J. G. Early, H. E. Burdette, *J. Appl. Cryst.*, **7**, 535 (1974).
8. A. K. Freund, Nucl. Instr. and Meth., **124**, 93 (1975).
9. J. R. Schneider, *J. Appl. Cryst.*, **7**, 541 (1974).
10. J. R. Schneider, *J. Appl. Cryst.*, **7**, 547 (1974).
11. T. Wroblewski, 2nd European Conference on Progress in X-Ray Synchrotron Radiation Research, Bologna 1990, (1990).
12. A. K. Freund, Nuclear Instruments and Methods in Physics Research, **A238**, 570 (1985).
13. S. Jönsson, A. Freund, F. Aldinger, *Metall*, **12**, 1257 (1979).
14. F. Mücklich, U. Scholz, G. Plachke, G. Petzow, to be published.
15. F. Mücklich, U. Scholz, Z. Nikolic, W. Yuan, G. Feldhofer, G. Petzow, to be published.
16. P. Hartmann, I. Sunagawa (Ed.), "Modern PBC Theory" in Morphology of Crystals, Part A (Terra Scientific Publ., Tokyo, 1987), 269.
17. G. Müller, R. Rupp, Crystal Properties and Preparation, **35**, 138 (1991).
18. A. T. Dinsdale, CALPHAD, **15**, **4**, 319 (1991).
19. G. Petzow, F. Aldinger, S. Jönsson, O. Preuss, "Beryllium and Beryllium Compounds", in: Ullmann's Encyclopedia of Industrial Chemistry (VCH Verlagsgesellschaft mbH, Weinheim, 1985), vol. A4.
20. R. Hultgren, R. L. Orr, K. K. Kelley, Supplement Values of Thermodynamic Properties of Metals and Alloys (University of California, Berkeley, 1972).
21. A. J. Martin, A. Moore, *Journal of the Less-Common Metals*, **1**, 85 (1959).
22. F. Zontone, J. Baruchel, X-ray topographic analysis of Beryllium crystals (International Report, European Synchrotron Radiation Facility, 1992).
23. J. Als-Nielsen, A. K. Freund, Rev. Sci. Instr., to be published.
24. A. K. Freund, St. Joksch, H. Kawata, G. Marot, E. Ziegler, Rev. Sci. Instr., to be published.
25. D. Webster, G. J. London, *Beryllium Science and Technology* (Plenum Press, New York London, 1979), vol. 2.
26. R. Le Hazif, G. Edelin, J. M. Dupoy, *Metallurgical Transactions*, **4**, 1275 (1973).
27. D. S. Gelles, H. L. Heinisch, 5th International Conference on Fusion Reactor Materials, Nov. 17–22, 1991, Clearwater, FL. (1991).
28. F. Mücklich, S. Mücklich, W. Sigle, G. Petzow, to be published.
29. G. Petzow, F. Mücklich, S. Mücklich, GER, 41 31 404.2, (1991).
30. D. Hull, D. J. Bacon, *Introduction to Dislocations* (International Series on Materials Science and Technology) (Pergamon Press, Liverpool, 1984). vol. 37, 112.
31. M. Wilkens, *J. Appl. Cryst.*, **8**, 191 (1975).
32. A. K. Freund, *J. Appl. Cryst.*, **8**, 194 (1975).